2 Light Scattering and Absorption by Nonspherical Ice Crystals

Ping Yang and Kuo-Nan Liou

2.1 Introduction

The majority of ice crystals in the atmosphere exist in cirrus clouds, clouds that normally reside in the upper troposphere in midlatitudes. In the tropics, ice clouds associated with deep cumulus convections (Houze, 1993) can extend to the lower stratosphere. Ice crystals have also been frequently observed in the polar regions because of low temperatures. The global cirrus cover has been estimated to be about 20% to 25%, but recent analysis using the 15-μm CO_2 satellite channels has shown that their occurrence frequency can be larger than 50% in the tropics (Wylie *et al.*, 1994). The inclusion of the 1.375-μm water vapor absorption channel (Gao and Kaufman, 1995) in the recent Moderate Resolution Imaging Spectroradiometer (MODIS) instrument on Terra and Acqua satellite platforms (King *et al.* 2003) has offered an unprecedented opportunity to detect optically thin cirrus. However, many thin and subvisual cirrus clouds could have been missed from the implementation of various past and current passive satellite detection techniques.

From analysis of the MODIS images acquired from the visible and 1.375-μm channels, it has been shown that most clear-sky pixels identified by the visible channels actually contain thin cirrus (Roskovensky and Liou, 2003; Dessler and Yang, 2003; Meyer *et al.*, 2004). Because of their high location in the atmosphere and the complex microphysical properties of ice crystals within them, cirrus clouds differ significantly from low and middle clouds in terms of their radiative properties. High cirrus clouds reflect a portion of the incoming sunlight, referred to as the solar albedo effect. But at the same time these clouds can also effectively trap a significant amount of the thermal infrared radiation emitted from the surface and lower atmosphere, referred to as the infrared greenhouse effect (Liou, 1992). The intrinsic radiative properties of cirrus clouds determine the competition between the solar albedo and infrared greenhouse effects (Liou, 1986; Stephens *et al.*, 1990), essential to the discussion of the Earth's climate and climate change. Moreover, cirrus clouds are closely related to the water vapor distribution near the upper troposphere and the lower stratosphere (Jensen *et al.*, 1996; Holton and Gettelman, 2001). The important roles of cirrus clouds in

various atmospheric processes have been discussed by Liou (1986, 1992) as well as in a number of recent studies (see Lynch *et al.*, 2002).

Ice crystals in cirrus clouds are almost exclusively nonspherical particles (e.g., Heymsfield and Iaquinta, 2000), ranging from plates, solid and hollow columns, bullet rosettes, and aggregates, to more irregular shapes with various complex surface morphological conditions (e.g., surface roughness). The effect of nonspherical ice crystals within cirrus clouds on their bulk radiative properties is pronounced and must be accounted for in the development of remote sensing techniques and climate analysis. Liou *et al.* (2000) demonstrated that the approximation of nonspherical ice crystals as equivalent ice spheres for the single-scattering and radiative transfer processes can substantially underestimate the albedo of the cirrus. Moreover, the single-scattering properties associated with proper ice crystal morphologies must be used for a correct interpretation of other bulk optical properties of cirrus clouds, particularly, the polarization configuration (Liou and Takano, 2002). Mishchenko *et al.* (1996), Rolland *et al.* (2000), and Yang *et al.* (2001a) also showed strong sensitivity of the cirrus cloud albedo, bidirectional reflectance, and the accuracy of optical thickness retrieval to the ice particle shape assumed. Consequently, it is critically important that the nonsphericity of ice crystals be accurately modeled in radiative transfer computations and remote sensing implementations involving cirrus clouds.

Because of the importance of ubiquitous cirrus clouds in remote sensing and climate research, substantial efforts have been made in the last three decades to understand and determine the fundamental scattering and absorption properties of ice crystals. Early research efforts to account for the nonsphericity of ice crystals in cirrus can be traced back to the studies by Liou (1972a, 1972b) and Stephens (1980a, 1980b) who assumed that these clouds are composed of long circular cylinders. The analytical solution for the scattering of light by an infinite circular cylinder at normal incidence was developed by Lord Rayleigh (1918). Wait (1955), Kerker (1969), and Liou (1972a) extended the solutions for oblique incidence. The single-scattering properties of ice crystals assuming circular-cylinder shape, however, cannot be used to explain a number of optical phenomena associated with cirrus clouds, for example, the well-known 22° halo. The simplest habits (or shapes) of realistic ice crystals are columns and plates with well-defined hexagonal structures. Even for this type of ice crystal, it appears not to be possible to impose an appropriate coordinate system to analytically solve the associated electromagnetic wave equation subjected to the boundary conditions at the surface of a hexagonal particle. The difficulty in conjunction with the application of the variable separation method to complex ice crystal morphologies (e.g., bullet rosettes and aggregates) would be more prominent. This is because proper coordinate systems for the variable separation method can only be defined in cases involving the scattering of light by spheres (Lorenz, 1890; Mie, 1908), spheroids (Oguchi, 1973; Asano and Yamamoto, 1975), and infinite cylinders (Kerker, 1969; Liou, 1972a).

From the late 1970s to the 1990s, the geometric optics method by means of the ray-tracing technique has been extensively used to investigate the single-scattering properties of nonspherical ice crystals (Wendling *et al.*, 1979; Coleman

and Liou, 1981; Cai and Liou, 1982; Takano and Jayaweera, 1985; Takano and Liou, 1989a, 1989b; Macke, 1993; Hess and Wiegner, 1994; Macke *et al.*, 1996a). Note that application of the ray-tracing technique to light scattering by a sphere and a hexagonal column can be traced back to the study by Liou and Hansen (1971) and Jacobowitz (1971), respectively. The research results from these efforts have been used in various applications in conjunction with the study of cirrus clouds, ranging from remote sensing (e.g. Minnis *et al.*, 1993a, 1993b) to the parameterization of the radiative properties of ice clouds (Ebert and Curry, 1992; Fu and Liou, 1993) for use in climate models.

Recent reviews by Wriedt (1998), Kokhanovsky (1999), Mishchenko *et al.* (2000), Liou (2002), and Kahnert (2003) have enumerated various methods that have been developed for the solution of light scattering by nonspherical particles. These include the T-matrix method (Waterman, 1971; Mishchenko and Travis, 1998), the discrete dipole approximation (Purcell and Pennypacker, 1973; Draine and Flatau, 1994), the finite-difference time domain (FDTD) method (Yee, 1966; Taflove and Brodwin, 1975; Holland, 1977; Kunz and Lee, 1978; Taflove, 1980; Kunz and Simpson, 1981; Umashankar and Taflove, 1982; Taflove, and Umashankar, 1990; Yang and Liou, 1996a; Yang *et al.*, 2000; Sun *et al.*, 1999), and the boundary-element method (Miller, 1988; Kress, 1990; Mano, 2000), and various approximate methods including the geometric optics approximation. Applications of some of these methods to light scattering by ice crystals have been shown to be useful for a better understanding of the optical and radiative properties of cirrus clouds.

In this chapter, we review the progress in the studies of the scattering and absorption properties of nonspherical ice crystals in the Earth's atmosphere from the theoretical and computational perspectives. Specifically, we will highlight the method of geometric optics and the relevant improvements based on which ray-tracing can be performed for large ice crystals with complex geometries and the FDTD numerical method that can be used for the solution of light scattering by small nonspherical and inhomogeneous ice crystals. No originality is claimed in this review; however, we have made an effort to systematically recapture the geometric optics approach and illustrate the basic concepts of the FDTD method and the major numerical steps associated with its application to light scattering and absorption by ice crystals.

2.2 Geometric Optics for Light Scattering by Large Ice Crystals

According to aircraft observations (e.g., Mitchell *et al.*, 1996; McFarquhar *et al.*, 1999) by means of the optical imaging, high resolution video camera, and replicator techniques, the ice crystal size distribution in various types of cirrus clouds ranges from about 10 micrometers to thousands of micrometers. For visible and near-infrared wavelengths, the size parameters (defined as $\pi D/\lambda$ in which D and λ are the particle's characteristic dimension and the incident wavelength, respectively) associated with these particles are large enough that we may apply the

principles of geometric optics in terms of the ray-tracing technique. van de Hulst (1957) and Liou and Hansen (1971) applied this technique to light scattering by spheres. The latter authors also compared the phase function and polarization patterns computed from the geometric ray-tracing method and the Lorenz–Mie theory for polydisperse spheres. The solution from the ray-tracing technique is reasonably accurate when the modal size parameter is larger than 100 for a polydisperse system of spheres. The earliest application of ray-tracing to light scattering by hexagonal ice prisms was first carried out by Jacobowitz (1971). In his study, a sufficiently large number of equally spaced, parallel rays were traced through a hexagonal ice crystal. The external reflection and two refractions after various orders of internal reflections were summed to determine the scattering pattern in the far field. Diffraction contribution to the scattering of the incident radiation in the forward direction can be computed by Kirchhoff's formula. In Jacobowitz's study, hexagonal prisms were assumed to be infinite by long, which is not realistic. To circumvent this shortcoming, Wendling *et al.* (1979) combined the Monte Carlo method and the ray-tracing technique to compute the phase function of finite hexagonal columns. In these early studies, the polarization effect and phase interferences associated with the incident, internal, and scattered rays were not accounted for in the calculation.

Cai and Liou (1982) were the first to include the polarization configuration and phase interferences in ray-tracing to compute the single-scattering properties of hexagonal columns and plates. The theoretical foundation for the 'conventional' geometric ray tracing and the associated computional algorithm developed by Cai and Liou (1982) were later improved and refined by a number of researchers. Takano and Liou (1989a, 1989b) considered the effects of the ice crystal's birefringence property, horizontal orientation, and size spectrum in association with light scattering calculations. The single-scattering properties of ice crystals with horizontally orientation have also been investigated by Rockwitz (1989) and Noel *et al.* (2001). The ray-tracing method has been applied to various complex ice crystal shapes by Takano and Liou (1995), Macke (1993), Macke *et al.* (1996a), Iaquinta *et al.* (1995), Muinonen *et al.* (1997), Peltoniemi *et al.* (1998), and Yang and Liou (1998), and to ice crystals with inclusions (e.g., air bubbles and soots) by Macke *et al.* (1996b) and Macke (2000). Application of the ray-tracing technique implemented with the Monte Carlo method to complex geometries have also been recently reported by Nousiainen *et al.* (2003), and Grynko and Shkuratov (2003). Most recently, Borovoi *et al.* (2002) investigated the scattering characteristics (backscattering features, in particular) of hexagonal ice crystals with arbitrary orientations using the ray-tracing method. Additionally, Borovoi and Grishin (2003) reported an effective ray-tracing algorithm for computing the Jones scattering matrix, and subsequently, the Mueller matrix.

Alternate approaches to the conventional ray-tracing method have been developed by Muinonen (1989) and Yang and Liou (1995, 1996b, and 1997) in which the principles of geometric optics are applied to the computation of the nearfield either on the surface of or inside the scattering particle. The near field obtained from the ray-tracing technique is then mapped to the far field on the

basis of either a surface-integral- or a volume-integral-based electromagnetic relation. Below we systematically recast the theoretical basis of the conventional ray-tracing technique, and follow with a concise presentation of two versions of the improved geometric optics method for the scattering of light by ice crystals.

The ray-tracing algorithm for the scattering of polarized light by nonspherical ice crystals that was formulated by Cai and Liou (1982) used various specific coordinate systems. To simplify the formulation presented in this paper, we shall adopt a vector form (Yang and Cai, 1990; Yang and Liou, 1996b, 1997) that is independent of specific coordinate systems. As shown in Fig. 2.1, when the size parameter associated with the scattering particle is large, the incident field can be thought of as composing of a bundle of localized waves or rays. As articulated in Cai and Liou (1982), the width of localized rays must be much larger than the incident wavelength and yet smaller than the ice crystal size.

Consider an incident ray that passes through point Q_0 and propagates along the incident direction specified by a unit vector $\hat{e}_0^{\mathrm{i}}$. The ray first impinges on the particle surface at point Q_1 where external reflection and refraction occur. For reflection and refraction at this incident point, the directions of the incident, reflected, and refracted rays are denoted by the unit vectors $\hat{e}_1^{\mathrm{i}}$, $\hat{e}_1^{\mathrm{r}}$, and $\hat{e}_1^{\mathrm{t}}$, re-

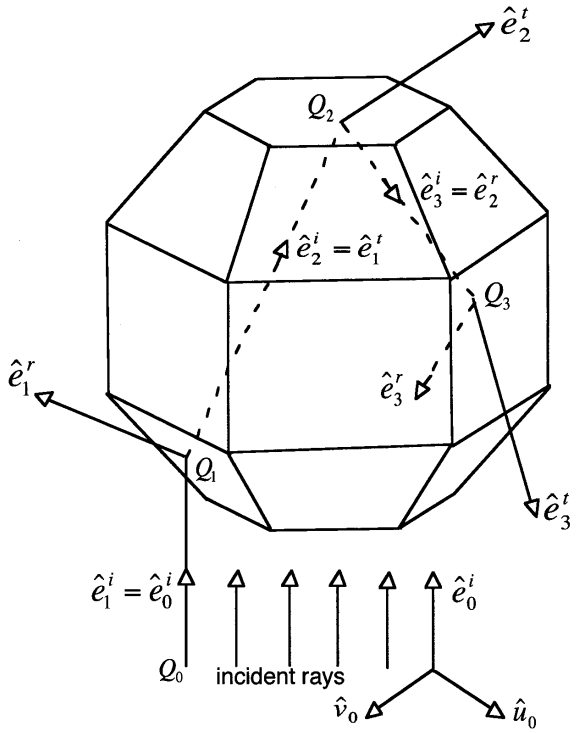

Fig. 2.1. A conceptual diagram for the principle of the ray-tracing technique for computing the single-scattering properties of a particle that is much larger than the incident wavelength.

spectively. The first-order refracted ray then impinges on the next incident point at Q_2 where the first-order internal reflection and the corresponding refraction occur. Note that for the incidence at the point Q_2, the incident direction $\hat{e}_2^{\rm i}$ is the same as that of the first-order refracted ray. Likewise, the subsequent internal reflections and refractions occur at the points $Q_{\rm p}$ in which the order of the ray, p, is larger than 2. The tracing of a ray can be terminated when the energy carried by this ray is practically negligible.

To trace the reflected and refracted rays, let $\hat{n}_{\rm p}$ ($p = 1, 2, 3, \ldots$) be the unit vectors locally normal to the particle surfaces at the incident points $Q_{\rm p}$ ($p = 1, 2, 3, \ldots$) facing the incoming rays, as shown in Fig. 2.2. For the external reflection at the point Q_1, the incident direction $\hat{e}_1^{\rm i}$ and the incident angle $\theta_1^{\rm i}$ are given, respectively, by the following two expressions:

$$\hat{e}_1^{\rm i} = \hat{e}_0^{\rm i}, \tag{2.1}$$

$$\theta_1^{\rm i} = \cos^{-1}(-\hat{n}_1 \cdot \hat{e}_1^{\rm i}), \tag{2.2}$$

where $\hat{e}_0^{\rm i}$ denotes the initial incident direction (Fig. 2.1). Following Snell's law, the directions of the externally reflected ray and the corresponding refracted ray are defined by

$$\hat{e}_1^{\rm r} = \hat{e}_1^{\rm i} + 2\cos\theta_1^{\rm i}\hat{n}_1, \tag{2.3}$$

$$\hat{e}_1^{\rm t} = \hat{e}_1^{\rm i}/m + (\cos\theta_1^{\rm i}/m - \cos\theta_1^{\rm t})\hat{n}_1, \tag{2.4}$$

where m is the refractive index of the scattering particle, and $\theta_1^{\rm t}$ is the refractive angle given by Snell's law as follows:

$$\theta_1^{\rm t} = \sin^{-1}(\sin\theta_1^{\rm i}/m). \tag{2.5}$$

When the refractive index, m, is a complex number, simultaneous absorption and scattering occur and the refracted wave within the particle is an inhomogeneous wave (Born and Wolf, 1959; Bohren and Huffman, 1983). In this case,

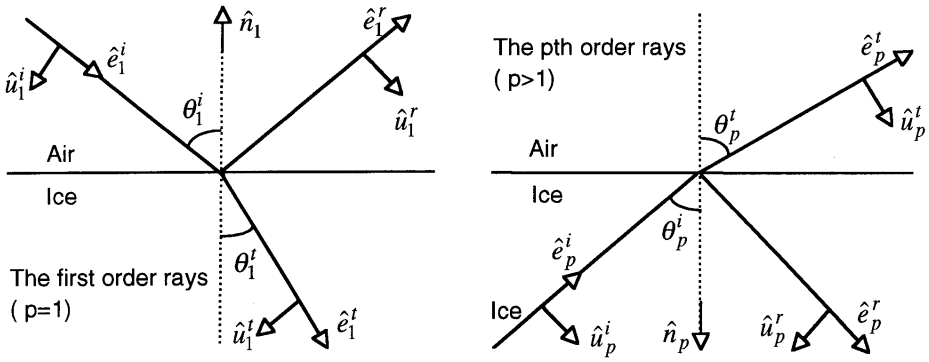

Fig. 2.2. Schematic diagrams for the directions of the incident, reflected and refracted rays. Also shown are the unit vectors for specifying the polarization configuration. Note that $\hat{v}_1$ and $\hat{v}_p$ (not shown in the diagram) point out of the paper.

an adjusted refractive must be used to trace the refracted rays (Yang and Liou, 1995). Note that Born and Wolf (1959) only formulated the Fresnel formula by avoiding the complex refraction angle when absorption occurs. Yang *et al.* (2001b) showed that in general the electric field vector associated with the refracted rays may not be perpendicular to the ray direction and developed an improved scheme for the ray-tracing computation. For practical computations at the visible and near-infrared wavelengths, the real part of the refractive index may be used as an excellent approximation of the adjusted refractive index for tracing the ray directions on the basis of eqs (2.4) and (2.5). The issue associated with the inhomogeneous wave properties within an ice crystal involving complex refractive index will not be elaborated further. Interested readers in this subject may wish to consult with the work of Born and Wolf (1959), Bohren and Huffman (1983), Dupertuis *et al.* (1994), Yang and Liou (1995), Yang *et al.* (2001b), Liou (2002), and Chang *et al.* (2005).

For internal reflection with orders of $p = 2, 3, 4, \ldots$, the incident directions can be defined in a likely manner and are given by the directions of either the first-order refracted rays or internally reflected rays as follows:

$$\hat{e}_2^{\mathrm{i}} = \hat{e}_1^{\mathrm{t}}, \tag{2.6}$$

$$\hat{e}_{\mathrm{p}}^{\mathrm{i}} = \hat{e}_{\mathrm{p}-1}^{\mathrm{r}}, \; p = 3, 4, 5, \ldots \tag{2.7}$$

With some vector algebraic manipulations on the basis of Snell's law, it can be shown that the propagating directions of the pth order reflected and refracted rays are given by

$$\hat{e}_{\mathrm{p}}^{\mathrm{r}} = \hat{e}_{\mathrm{p}}^{\mathrm{i}} + 2\cos\theta_{\mathrm{p}}^{\mathrm{i}}\hat{n}_{\mathrm{p}}, \tag{2.8}$$

$$\hat{e}_{\mathrm{p}}^{\mathrm{t}} = m\hat{e}_{\mathrm{p}}^{\mathrm{i}} + (m\cos\theta_{\mathrm{p}}^{\mathrm{i}} - \cos\theta_{\mathrm{p}}^{\mathrm{t}})\hat{n}_{\mathrm{p}}, \tag{2.9}$$

where the incident and refraction angles, $\theta_{\mathrm{p}}^{\mathrm{i}}$ and $\theta_{\mathrm{p}}^{\mathrm{t}}$, are defined via the following expressions:

$$\theta_{\mathrm{p}}^{\mathrm{i}} = \cos^{-1}(-\hat{n}_{\mathrm{p}} \cdot \hat{e}_{\mathrm{p}}^{\mathrm{i}}), \tag{2.10}$$

$$\theta_{\mathrm{p}}^{\mathrm{t}} = \sin^{-1}(m\sin\theta_{\mathrm{p}}^{\mathrm{i}}). \tag{2.11}$$

The total reflection occurs if the term $m\sin\theta_{\mathrm{p}}^{\mathrm{i}}$ in eq. (2.11) is larger than 1. In this case, a refracted ray should not be expected and the ray-tracing computation should be continued only for the ray associated with total reflection. Equations (2.1)–(2.11) constitute a closed set of equations for tracing the directions of all the reflected and refracted rays associated with a given incident ray.

A localized plane electromagnetic wave is a transverse vector wave. Thus, the vector property or the polarization configuration of the electric fields associated with localized rays in the ray-tracing computation must be accounted for. To include the polarization configuration, we shall define various auxiliary unit vectors. For the incident direction of an initial ray specified by a unit vector $\hat{e}_0^{\mathrm{i}}$, we define two unit vector $\hat{u}_0$ and $\hat{v}_0$ (see Fig. 2.1) that are normal to the incident direction and satisfy the relations as follows:

$$\hat{u}_0 \cdot \hat{v}_0 = 0 \text{ and } \hat{v}_0 \times \hat{u}_0 = \hat{e}_0^{\mathrm{i}}. \tag{2.12}$$

The unit vectors $\hat{v}_0$, $\hat{u}_0$ and $\hat{e}_0^{\mathrm{i}}$ defined in this equation constitute a right-handed coordinate system. To define the initial rays in practice, we may specify the unit vectors $\hat{v}_0$, $\hat{u}_0$ and $\hat{e}_0^{\mathrm{i}}$ to point to the directions along the x-, y- and z-axis of the incident coordinate system. Because the unit vectors $\hat{e}_0^{\mathrm{i}}$, $\hat{u}_0$ and $\hat{v}_0$ are orthogonal to each other, the incident polarization configuration can be specified with respect to $\hat{u}_0$ and $\hat{v}_0$, that is, the incident electric field $\boldsymbol{E}_0^{\mathrm{i}}$ can be written as follows:

$$\boldsymbol{E}_0^{\mathrm{i}} = E_{0u}^{\mathrm{i}} \hat{u}_0 + E_{0v}^{\mathrm{i}} \hat{v}_0. \tag{2.13}$$

Similarly, we may define three pairs of unit vectors, $(\hat{u}_p^{\mathrm{i}}, \hat{v}_p)$, $(\hat{u}_p^{\mathrm{r}}, \hat{v}_p)$, and $(\hat{u}_p^{\mathrm{t}}, \hat{v}_p)$ for the ray directions along $\hat{e}_p^{\mathrm{i}}$, $\hat{e}_p^{\mathrm{r}}$ and $\hat{e}_p^{\mathrm{t}}$ ($p = 1, 2, 3, \ldots$), respectively. The unit vectors $\hat{u}_p^{\mathrm{i}}$, $\hat{u}_p^{\mathrm{r}}$ and $\hat{u}_p^{\mathrm{t}}$ point along the directions shown in Fig. 2.2, if the unit vectors, $\hat{v}_p$, $p = 1, 2, 3, \ldots$, (not shown in Fig. 2.2) are defined as being pointed out of the paper. These vectors can be specified via the following expressions:

$$\hat{v}_p = (\hat{e}_p^{\mathrm{i}} \times \hat{n}_p)/\sin\theta_p^{\mathrm{i}}, \ p = 1, 2, 3, \ldots, \tag{2.14}$$

$$\hat{u}_p^{\mathrm{i,r,t}} = \hat{e}_p^{\mathrm{i,r,t}} \times \hat{v}_p, \ p = 1, 2, 3, \ldots. \tag{2.15}$$

Evidently, the unit vector $\hat{v}_p$ is normal to the incident plane, the plane containing the incident direction and the direction locally normal to the particle surface at the incident point, for the pth-order reflection and refraction. The unit vectors $\hat{u}_p^{\mathrm{i}}$, $\hat{u}_p^{\mathrm{r}}$, and $\hat{u}_p^{\mathrm{t}}$ are parallel to the pth-order incident plane. Note that $\hat{v}_p$ in eq. (2.14) cannot be uniquely specified if $\sin\theta_p^{\mathrm{i}} = 0$. In this case, we select $\hat{v}_p = \hat{v}_{p-1}$. With the aforementioned unit vectors defined, the electric fields associated with the pth-order incident, reflected, and refracted rays can be expressed as follows:

$$\boldsymbol{E}_p^{\mathrm{i,r,t}} = E_{pu}^{\mathrm{i,r,t}} \hat{u}_p^{\mathrm{i,r,t}} + E_{pv}^{\mathrm{i,r,t}} \hat{v}_p. \tag{2.16}$$

Consider now the external reflection and the first-order refraction. In order to apply the Fresnel formulas, the electric field associated with the incident ray impinging on the point Q_1 must be specified with respect to $\hat{u}_1^{\mathrm{i}}$ and $\hat{v}_1$. Also, the electric field associated with the incident ray specified in eq. (2.13) can also be expressed in an alternative form as follows:

$$\boldsymbol{E}_0^{\mathrm{i}} = E_{1u}^{\mathrm{i}} \hat{u}_1^{\mathrm{i}} + E_{1v}^{\mathrm{i}} \hat{v}_1. \tag{2.17}$$

Equations (2.13) and (2.17) for the incident electric vector are related via a rotational matrix in the form

$$\begin{pmatrix} E_{1u}^{\mathrm{i}} \\ E_{1v}^{\mathrm{i}} \end{pmatrix} = \varGamma_1 \begin{pmatrix} E_{0u}^{\mathrm{i}} \\ E_{0v}^{\mathrm{i}} \end{pmatrix}, \tag{2.18}$$

where $\varGamma_1$ is a rotational matrix given by

$$\varGamma_1 = \begin{pmatrix} \hat{u}_1^{\mathrm{i}} \cdot \hat{u}_0 & \hat{u}_1^{\mathrm{i}} \cdot \hat{v}_0 \\ \hat{v}_1 \cdot \hat{u}_0 & \hat{v}_1 \cdot \hat{v}_0 \end{pmatrix}. \tag{2.19}$$

Because the field components on the left-hand side of eq. (2.18) are specified with respect to the incident plane, the Fresnel formulas can be applied. The externally reflected field ($\boldsymbol{E}_1^{\mathrm{r}}$) is given by

$$\boldsymbol{E}_1^{\mathrm{r}} = E_{1u}^{\mathrm{r}}\hat{u}_1^{\mathrm{r}} + E_{1v}^{\mathrm{r}}\hat{v}_1, \tag{2.20}$$

where

$$\begin{pmatrix} E_{1u}^{\mathrm{r}} \\ E_{1v}^{\mathrm{r}} \end{pmatrix} = R_1 \begin{pmatrix} E_{1u}^{\mathrm{i}} \\ E_{1v}^{\mathrm{i}} \end{pmatrix} = R_1 \Gamma_1 \begin{pmatrix} E_{0u}^{\mathrm{i}} \\ E_{0v}^{\mathrm{i}} \end{pmatrix}. \tag{2.21}$$

In eq. (2.21), R_1 is the reflection matrix for the external reflection given by

$$R_1 = \begin{pmatrix} R_{1u} & 0 \\ 0 & R_{1v} \end{pmatrix}. \tag{2.22}$$

The elements of the reflection matrix in eq. (2.22) are given by the Fresnel coefficients (Born and Wolf, 1959) as follows:

$$R_{1u} = \frac{m\,\cos\theta_1^{\mathrm{i}} - \cos\theta_1^{\mathrm{t}}}{m\,\cos\theta_1^{\mathrm{i}} + \cos\theta_1^{\mathrm{t}}}, \tag{2.23}$$

$$R_{1v} = \frac{\cos\theta_1^{\mathrm{i}} - m\,\cos\theta_1^{\mathrm{t}}}{\cos\theta_1^{\mathrm{i}} + m\,\cos\theta_1^{\mathrm{t}}}. \tag{2.24}$$

Similarly, the electric field associated with the first-order refracted ray is given by

$$\boldsymbol{E}_1^{\mathrm{t}} = E_{1u}^{\mathrm{t}}\hat{u}_1^{\mathrm{t}} + E_{1v}^{\mathrm{t}}\hat{v}_1, \tag{2.25}$$

$$\begin{pmatrix} E_{1u}^{\mathrm{t}} \\ E_{1v}^{\mathrm{t}} \end{pmatrix} = T_1 \begin{pmatrix} E_{1u}^{\mathrm{i}} \\ E_{1v}^{\mathrm{i}} \end{pmatrix} = T_1 \Gamma_1 \begin{pmatrix} E_{0u}^{\mathrm{i}} \\ E_{0v}^{\mathrm{i}} \end{pmatrix}, \tag{2.26}$$

where the refraction matrix T_1 is defined in the form

$$T_1 = \begin{pmatrix} T_{1u} & 0 \\ 0 & T_{1v} \end{pmatrix} = \begin{pmatrix} (1 - R_{1u}^2)^{1/2} & 0 \\ 0 & (1 - R_{1v}^2)^{1/2} \end{pmatrix}. \tag{2.27}$$

In eq. (2.27), the conservation of the energy carried out by the ray due to a change in the refractive index and ray cross-section in two media is accounted for in the refraction matrix (see eq. (48) in Cai and Liou (1982) and references cited therein).

For the external reflection, the direction along the reflected ray is the scattering direction. Thus, the scattering angle is given by

$$\theta_1^{\mathrm{s}} = \cos^{-1}(\hat{e}_0^{\mathrm{i}} \cdot \hat{e}_1^{\mathrm{r}}). \tag{2.28}$$

The direction that is perpendicular to the scattering plane can be specified by

$$\hat{v}_1^{\mathrm{s}} = \hat{e}_0^{\mathrm{i}} \times \hat{e}_1^{\mathrm{r}} / \sin\theta_1^{\mathrm{s}}. \tag{2.29}$$

If $\sin\theta_1^{\mathrm{s}} = 0$ in eq. (2.29), implying the forward (i.e., $\theta_1^{\mathrm{s}} = 0^\circ$) and backward scattering (i.e., $\theta_1^{\mathrm{s}} = 180^\circ$), the vector $\hat{v}_1^{\mathrm{s}}$ cannot be defined. In this case, we

select $\hat{v}_1^{\rm s} = \hat{v}_0$. After the unit vector $\hat{v}_1^{\rm s}$ is defined, the direction parallel to the scattering plane is given by

$$\hat{u}_1^{\rm s} = \hat{e}_1^{\rm r} \times \hat{v}_1^{\rm s}. \tag{2.30}$$

If we express the electric field associated with the externally reflected ray with respect to two directions parallel and perpendicular to the scattering plane, we have

$$\boldsymbol{E}_1^{\rm r} = E_{1u}^{\rm s}\hat{u}_1^{\rm s} + E_{1v}^{\rm s}\hat{v}_1^{\rm s}. \tag{2.31}$$

From eqs (2.20), (2.21) and (2.31), it follows that

$$\begin{pmatrix} E_{1u}^{\rm s} \\ E_{1v}^{\rm s} \end{pmatrix} = \varGamma_1^{\rm s} R_1 \varGamma_1 \begin{pmatrix} E_{0u}^{\rm i} \\ E_{0v}^{\rm i} \end{pmatrix}, \tag{2.32}$$

where $\varGamma_1^{\rm s}$ is a rational matrix, given by

$$\varGamma_1^{\rm s} = \begin{pmatrix} \hat{u}_1^{\rm s}\cdot\hat{u}_1^{\rm r} & \hat{u}_1^{\rm s}\cdot\hat{v}_1 \\ \hat{v}_1^{\rm s}\cdot\hat{u}_1^{\rm r} & \hat{v}_1^{\rm s}\cdot\hat{v}_1 \end{pmatrix}. \tag{2.33}$$

To obtain the scattering matrix, the incident field must be specified with respect to the directions parallel and perpendicular to the scattering plane, that is, the incident field needs to be in the form

$$\boldsymbol{E}_0^{\rm i} = E_{1su}^{\rm i}(\hat{e}_0^{\rm i} \times \hat{v}_1^{\rm s}) + E_{1sv}^{\rm i}\hat{v}_1^{\rm s}. \tag{2.34}$$

Note that the unit vector $\hat{e}_0^{\rm i} \times \hat{v}_1^{\rm s}$ in eq. (2.34) is parallel to the scattering plane. The expression in eq. (2.34) for the incident field is related to that in eq. (2.13) as follows:

$$\begin{pmatrix} E_{0u}^{\rm i} \\ E_{0v}^{\rm i} \end{pmatrix} = \varGamma_1^{\rm i} \begin{pmatrix} E_{1su}^{\rm i} \\ E_{1sv}^{\rm i} \end{pmatrix}, \tag{2.35}$$

where $\varGamma_1^{\rm i}$ is a 2-D rotational matrix given by

$$\varGamma_1^{\rm i} = \begin{pmatrix} \hat{u}_0\cdot(\hat{e}_0^{\rm i}\times\hat{v}_1^{\rm s}) & \hat{u}_0\cdot\hat{v}_1^{\rm s} \\ \hat{v}_0\cdot(\hat{e}_0^{\rm i}\times\hat{v}_1^{\rm s}) & \hat{v}_0\cdot\hat{v}_1^{\rm s} \end{pmatrix}. \tag{2.36}$$

Thus, we can express the scattered field in eq. (2.32) as follows:

$$\begin{pmatrix} E_{1u}^{\rm s} \\ E_{1v}^{\rm s} \end{pmatrix} = \varGamma_1^{\rm s} R_1 \varGamma_1 \varGamma_1^{\rm i} \begin{pmatrix} E_{1su}^{\rm i} \\ E_{1sv}^{\rm i} \end{pmatrix}. \tag{2.37}$$

Similarly, for the refracted rays with $p = 2$, we have

$$\begin{pmatrix} E_{2u}^{\rm s} \\ E_{2v}^{\rm s} \end{pmatrix} = \varGamma_2^{\rm s} T_2 \varGamma_2 T_1 \varGamma_1 \varGamma_2^{\rm i} \begin{pmatrix} E_{2su}^{\rm i} \\ E_{2sv}^{\rm i} \end{pmatrix}. \tag{2.38}$$

For the orders $p = 3, 4, 5, \ldots$, we have

$$\begin{pmatrix} E_{pu}^{\rm s} \\ E_{pv}^{\rm s} \end{pmatrix} = \varGamma_p^{\rm s} T_p \varGamma_p \cdots R_2 \varGamma_2 T_1 \varGamma_1 \varGamma_p^{\rm i} \begin{pmatrix} E_{psu}^{\rm i} \\ E_{psv} \end{pmatrix}. \tag{2.39}$$

The definitions for Γ_p^{s}, T_p, Γ_p, R_p, and Γ_p^{i} are similar to those for the case with $p = 1$. In this manner, both the incident and scattered electric field vectors are expressed with respect to the scattering plane in eqs (2.37)–(2.39). Thus, the contributions of the emerging or scattered rays to the amplitude scattering matrix can be expressed in the forms

$$A^{(1)} = \begin{pmatrix} A_2^{(1)} & A_3^{(1)} \\ A_4^{(1)} & A_1^{(1)} \end{pmatrix} = \Gamma_1^{\mathrm{s}} R_1 \Gamma_1 \Gamma_1^{\mathrm{i}}, \text{ for externally reflected rays,} \tag{2.40}$$

$$A^{(2)} = \begin{pmatrix} A_2^{(2)} & A_3^{(2)} \\ A_4^{(2)} & A_1^{(2)} \end{pmatrix} = \Gamma_2^{\mathrm{s}} T_2 \Gamma_2 T_1 \Gamma_1 \Gamma_2^{\mathrm{i}}, \text{ for second-order transmitted rays,} \tag{2.41}$$

$$A^{(3)} = \begin{pmatrix} A_2^{(3)} & A_3^{(3)} \\ A_4^{(3)} & A_1^{(3)} \end{pmatrix} = \Gamma_p^{\mathrm{s}} T_p \Gamma_p \cdots R_2 \Gamma_2 T_1 \Gamma_1 \Gamma_p^{\mathrm{i}}, \text{ for } p\text{th } (p > 2)\text{-order transmitted rays.} \tag{2.42}$$

In the foregoing discussion, we have not accounted for the phase change associated with the optical paths of rays. The rays incident on the scattering particle at different locations must experience phase change due to different paths. Noticing this feature, Cai and Liou (1982) considered the phase interference of the emerging rays in ray-tracing computations. Most follow-on studies reported in the literature essentially ignored the phase shifts associated with raypaths. However, it should be pointed out that the approach developed by Stamnes and Heier (1998) and Chen and Stamnes (1998) can also be used to effectively account for the phase inference of rays. Takano and Jayaweera (1985) showed that the phase interference can be smoothed out when ice crystals are randomly oriented. For practical applications, we normally assume the random orientation condition for ice crystals in radiative transfer computations. If ice crystals are horizontally oriented, the single-scattering properties depend not only on the scattering angle but also on the azimuth of the scattering plane. In this case, the radiative transfer calculation can be quite involved (Takano and Liou, 1989b). In addition to random orientation, the integration over the size spectrum will smooth out the fluctuations produced by phase interferences in the scattering pattern for one size.

For randomly oriented particles, the corresponding phase matrix has only six independent elements (van de Hulst, 1957). Thus, for the pth-order emerging ray, its contribution to the phase matrix is given by the following expression (Takano and Jayaweera, 1985):

$$F^{(\mathrm{p})} = \begin{pmatrix} (M_1^{(\mathrm{p})} + M_2^{(\mathrm{p})} + M_3^{(\mathrm{p})} + M_4^{(\mathrm{p})})/2 & (M_2^{(\mathrm{p})} - M_1^{(\mathrm{p})})/2 & 0 & 0 \\ (M_2^{(\mathrm{p})} - M_1^{(\mathrm{p})})/2 & (M_2^{(\mathrm{p})} - M_3^{(\mathrm{p})} - M_4^{(\mathrm{p})} + M_1^{(\mathrm{p})})/2 & 0 & 0 \\ 0 & 0 & S_{12}^{(\mathrm{p})} + S_{34}^{(\mathrm{p})} & -D_{12}^{(\mathrm{p})} \\ 0 & 0 & D_{21}^{(\mathrm{p})} & S_{12}^{(\mathrm{p})} - S_{34}^{(\mathrm{p})} \end{pmatrix}, \tag{2.43}$$

where the matrix $F^{(\mathrm{p})}$ transforms the incident Stokes parameters to the scattered Stokes parameters associated with the pth-order outgoing localized wave. In eq. (2.43), the phase matrix elements are defined by

$$M_{\rm i}^{(\rm p)} = |A_{\rm i}^{(\rm p)}|^2, \tag{2.44}$$

$$S_{ij}^{(\rm p)} = S_{ji}^{(\rm p)} = (A_I^{(\rm p)} A_j^{(\rm p)*} + A_i^{(\rm p)*} A_j^{(\rm p)})/2, \tag{2.45}$$

$$D_{ij}^{(\rm p)} = -D_{ji}^{(\rm p)} = \sqrt{-1}(A_i^{(\rm p)} A_j^{(\rm p)*} - A_i^{(\rm p)} A_j^{(\rm p)})/2, \tag{2.46}$$

where the subscripts i and j range from 1 to 4, and the asterisk indicates complex conjugate. Thus, the scattering matrix associated with the various orders of external reflections and transmissions of all the incident rays is given by

$$F_{\rm ray} = \sum_{j=1}^{N} \sum_{p=1}^{\infty} \Delta\sigma_j F_j^{(\rm p)} / \sum_{p=1}^{\infty} \Delta\sigma_j, \tag{2.47}$$

where j denotes that the external reflection and the various orders of transmission are associated with the jth initial ray, N is the total number of incident rays, and $\Delta\sigma_j$ is the cross-section of the jth initial ray. To speed up the computation, the foregoing ray-tracing algorithm can be implemented by using the Monte Carlo method. Interested readers may wish to consult with the papers by Wendling *et al.* (1979), Takano and Liou (1995), Macke (1993), and Yang and Liou (1998). More recently, an efficient algorithm for specifying the incident rays in the Monte Carlo ray-tracing technique implemented for convex geometries has been reported by Zhang *et al.* (2004).

In addition to the contributions from the reflected and refracted rays, diffraction also contributes to the scattering of the incident wave. According to Babinet's principle (Born and Wolf, 1959), the diffraction pattern associated with an object is the same as that for an aperture with a shape identical to the projection of the object on a plane normal to the incident direction. The diffraction matrix obtained by the scalar Fraunhofer diffraction theory for a scattering particle has been extensively employed in the previous ray-tracing studies. Yang and Liou (1998) showed that the scattering matrix associated with diffraction is given in the form

$$A_{\rm dif} = \frac{k^2}{2\pi} D \begin{bmatrix} (\cos\theta + \cos^2\theta)/2 & 0 \\ 0 & (1+\cos\theta)/2 \end{bmatrix}, \tag{2.48}$$

where

$$D = \iint_{\substack{\rm projected \\ \rm area}} \exp(-ik\hat{r}\cdot\bar{\xi})\, {\rm d}^2\xi. \tag{2.49}$$

From eqs (2.48) and (2.49), the contribution of diffraction to the scattering phase matrix, denoted as $F_{\rm dif}$, can be evaluated. To sum the contributions due to diffraction and Fresnel rays, proper weighting factors must be accounted for, particularly, in the case when the scattering particle is absorptive.

If the scattering ice crystal is absorptive, i.e., the imaginary refractive index is nonzero, the total absorption can be accounted for by considering the absorption of individual rays. In general, the absorption cross of a particle depends on the polarization configuration of the incident light. However, for randomly oriented particles, their absorption cross-section is the average of the absorption

cross-sections for two orthogonal polarization cases. Consider a case where the polarization of the incident light is specified as follows:

$$(\boldsymbol{E}^{\mathrm{i}}_{0u}, \boldsymbol{E}^{\mathrm{i}}_{0v}) = (1, 0). \tag{2.50}$$

The intensity of the first-order refracted field can be obtained from eq. (2.26) in the form

$$(\boldsymbol{E}^{\mathrm{t}}_{0u}, \boldsymbol{E}^{\mathrm{t}}_{0v})(\boldsymbol{E}^{\mathrm{t}}_{0u}, \boldsymbol{E}^{\mathrm{t}}_{0v})^{*,+}\Big|_{(\boldsymbol{E}^{\mathrm{i}}_{0u}, \boldsymbol{E}^{\mathrm{i}}_{0v})=(1,0)} = (1,0)(T_1\Gamma_1)^{+}(T_1\Gamma_1)^{*}(1,0)^{+}, \tag{2.51}$$

where the superscript symbol + denotes the transpose of a matrix, and $*$ indicates the complex conjugate. The intensity given by eq. (2.51) is essentially the amplitude of the Poyting vector (Born and Wolf, 1959) in which the refractive index and change in the ray cross-section due to refraction have been implicitly accounted for in the refractive matrix given by eq. (2.27). A similar expression can be derived for the case when the polarization of field is given by $(\boldsymbol{E}^{\mathrm{i}}_{0u}, \boldsymbol{E}^{\mathrm{i}}_{0v}) = (0, 1)$. Therefore, the contribution of the first-order refracted rays to the absorption cross-section is given by

$$\begin{aligned}
\sigma_{\mathrm{abs},1} &= \sum_{j=1}^{N} 2^{-1}\Delta\sigma_j \left[1 - \exp(-4\pi m_i d_{j1}/\lambda)\right] \\
&\quad \times \Big[(\boldsymbol{E}^{\mathrm{t}}_{pu}, \boldsymbol{E}^{\mathrm{t}}_{pv})(\boldsymbol{E}^{\mathrm{t}}_{\mathrm{pu}}, \boldsymbol{E}^{\mathrm{t}}_{\mathrm{pv}})^{*,+}\big|_{(\boldsymbol{E}^{\mathrm{i}}_{0u}, \boldsymbol{E}^{\mathrm{i}}_{0v})=(1,0)} \\
&\qquad + (\boldsymbol{E}^{\mathrm{t}}_{pu}, \boldsymbol{E}^{\mathrm{t}}_{pv})(\boldsymbol{E}^{\mathrm{t}}_{pu}, \boldsymbol{E}^{\mathrm{t}}_{pv})^{*,+}\big|_{(\boldsymbol{E}^{\mathrm{i}}_{0u}, \boldsymbol{E}^{\mathrm{i}}_{0v})=(1,0)}\Big] \\
&= \sum_{j=1}^{N} 2^{-1}\Delta\sigma_j \left[1 - \exp(-4\pi m_i d_{j1}/\lambda)\right] \\
&\qquad \cdot \left[(1,0)(T_1\Gamma_1)^{+}(T_1\Gamma_1)^{*}(1,0)^{+} + (0,1)(T_1\Gamma_1)^{+}(T_1\Gamma_1)^{*}(1,0)^{+}\right],
\end{aligned} \tag{2.52}$$

where subscript j denotes the jth initial ray, d_{j1} is the distance between the first incident point (i.e., Q_1 in Fig. 2.1) and the second incident point (i.e., Q_2 in Fig. 2.1), $\Delta\sigma_j$ is the cross-section of the jth initial ray, m_i is the imaginary part of the refractive index, and λ is the incident wavelength in a vacuum. Likewise, the contribution by the pth-order reflected rays is

$$\begin{aligned}
\sigma_{\mathrm{abs},p} &= \sum_{j=1}^{N} 2^{-1}\Delta\sigma_j \left[1 - \exp(-4\pi m_i d_{jp}/\lambda)\right] \exp\left(-4\pi m_i \lambda^{-1} \sum_{L=1}^{p-1} d_{jL}\right) \\
&\quad \times \Big[(1,0)(T_p\Gamma_p \cdots R_2\Gamma_2 t_1\Gamma_1)^{+}(T_p\Gamma_p \cdots R_2\Gamma_2 T_1\Gamma_1)^{*}(1,0)^{+} \\
&\quad + (0,1)(T_p\Gamma_p \cdots R_2\Gamma_2 T_1\Gamma_1)^{+}(T_p\Gamma_p \cdots R_2\Gamma_2 T_1\Gamma_1)^{*}(0,1)^{+}\Big],
\end{aligned} \tag{2.53}$$

Thus, the absorption cross-section of the scattering particle can be expressed as follows:

$$\sigma_{\rm abs} = \sum_{p=1}^{\infty} \sigma_{{\rm abs},p}. \tag{2.54}$$

In practice, the summation in eq. (2.54) can be truncated for the terms with $p > 10$, because the amount of the energy carried by the higher-order rays is insignificant. Equations (2.52)–(2.54) provide the explicit formulations for absorption cross-section within the framework of the ray-tracing technique in which the polarization configuration is fully accounted for. In the conventional ray-tracing method, the extinction cross-section is twice the projected area of the scattering particle, that is

$$\sigma_{\rm ext} = 2\sigma_p, \tag{2.55}$$

where σ_p is the particle's projected area on a plane normal to the incident direction. The contribution of diffraction to the extinction cross-section is equal to that associated with the externally reflected rays and the transmitted rays that experience two refractions and various orders of internal reflections.

One of the shortcomings of the conventional ray-tracing method is the production of the delta-transmission associated with the refraction of rays through two parallel faces of the pristine ice crystals. The delta-transmission phenomenon has been discussed in detail by Takano and Liou (1989a) and Mishchenko and Macke (1998). Let the portion of the scattering cross-section associated with the delta-transmission be σ_δ. Then, the scattering cross-section can be separated into three terms as follows:

$$\sigma_{\rm sca} = (\sigma_p - \sigma_{\rm abs} - \sigma_\delta) + \sigma_\delta + \sigma_p, \tag{2.56}$$

The first term $(\sigma_p - \sigma_{\rm abs} - \sigma_\delta)$ corresponds to the contribution from the externally reflected rays and the various transmitted rays excluding the delta-transmitted rays, the second term (σ_δ) denotes the contribution from the delta-transmitted rays, and the third term (σ_p) is associated with diffraction. Let f_δ be the ratio of the delta-transmitted energy to the total scattered energy defined by

$$f_\delta = \sigma_\delta/\sigma_{\rm sca} = \sigma_\delta/(2\sigma_p - \sigma_{\rm abs}) = \sigma_\delta/(\sigma_{\rm ext} - \sigma_{\rm abs}). \tag{2.57}$$

Using the standard notation, the scattered Stokes vector can be expressed as follows:

$$\begin{pmatrix} I_{\rm s} \\ Q_{\rm s} \\ U_{\rm s} \\ V_{\rm s} \end{pmatrix} = \frac{\sigma_{\rm sca}}{k^2 r^2} P \begin{pmatrix} I_{\rm i} \\ Q_{\rm i} \\ U_{\rm i} \\ V_{\rm i} \end{pmatrix}, \tag{2.58}$$

where $(I_{\rm i}, Q_{\rm i}, U_{\rm i}, V_{\rm i})$ and $(I_{\rm s}, Q_{\rm s}, U_{\rm s}, V_{\rm s})$ are the incident and scattered Stokes parameters, respectively, and P is the normalized phase matrix. Based on $F_{\rm ray}$ in eq. (2.47), $F_{\rm dif}$ that is defined on the basis of $A_{\rm dif}$ in eq. (2.48), the expressions in eqs (2.56) and (2.57), and the associated physical meanings of these quantities and expressions, the normalized phase matrix is given by

$$P(\theta) = \frac{[(2\sigma_p - \sigma_{\rm abs})(1-f_\delta) - \sigma_p] a F_{\rm ray} + 2(2\sigma_p - \sigma_{\rm abs}) f_\delta \delta(\cos\theta - 1)\bar{\bar{I}} + \sigma_p b F_{\rm dif}}{2\sigma_p - \sigma_{\rm abs}}$$
$$= 2 f_\delta \delta(\cos\theta - 1)\bar{\bar{I}} + \left[(1-f_\delta) - \frac{1}{2\tilde{\omega}_o}\right] a F_{\rm ray} + \frac{1}{2\tilde{\omega}_o} b F_{\rm dif}, \quad (2.59)$$

where $\tilde{\omega}_0 = \sigma_{\rm sca}/\sigma_{\rm ext}$ is the single-scattering albedo. In eq. (2.59) θ is the scattering angle, $\bar{\bar{I}}$ is a unit 4×4 matrix, and the two parameters, a and b, are normalization factors given, respectively, by the following two equations:

$$a = \frac{2}{\int_0^\pi F_{\rm ray,11}(\theta)\, \sin\theta \, {\rm d}\theta}, \quad (2.60)$$

$$b = \frac{2}{\int_0^\pi F_{\rm dif,11}(\theta)\, \sin\theta \, {\rm d}\theta}, \quad (2.61)$$

where the subscript 11 indicates the first element of the associated matrix. With the normalization factors given in eqs (2.60) and (2.61), it can be shown that the phase matrix in eq. (2.59) is normalized in the sense that the first phase matrix element P_{11} (i.e., the phase function) satisfies the following normalization condition:

$$\frac{1}{2}\int_0^\pi P_{11}(\theta) \sin\theta \, {\rm d}\theta = 1. \quad (2.62)$$

The conventional ray-tracing technique utilizes the assumption that the energy attenuated by a scattering particle is equally divided into two parts: extinction associated with diffraction and extinction due to Fresnel reflection and refraction. In this case, the extinction efficiency (i.e., the ratio of extinction cross-section to particle projected area) is 2 regardless of the size and shape of the scattering particle, referred to as the optical theorem. In addition, the computation of far field by directly applying the ray-tracing technique leads to the delta-transmission (Takano and Liou, 1989a) in the forward direction, as is evident from the presence of a delta function in eq. (2.59). To overcome these shortcomings, Yang and Liou (1995, 1996a, 1996b, 1997) have developed two improved geometric optics methods.

According to the fundamental theory of classic electrodynamics, the far field can be exactly computed if the tangential components of the electric and magnetic fields on the surface of a scattering particle are known (Jackson, 1998, p. 485) in the form

$$\boldsymbol{E}^{\rm s}(\boldsymbol{r})\big|_{kr\to\infty} = \frac{{\rm e}^{ikr}}{-ikr}\frac{k^2}{4\pi}\hat{r} \times \oint\!\!\!\!\!\!\int \{\hat{n}_{\rm s} \times \boldsymbol{E}(\boldsymbol{r}') - \hat{r} \times [\hat{n}_{\rm s} \times \mathbf{H}(\boldsymbol{r}')]\}\, {\rm e}^{-ik\hat{r}\cdot\boldsymbol{r}'}\, {\rm d}^2\boldsymbol{r}, \quad (2.63)$$

where the integral domain is the surface of the scattering particle. In essence, eq. (2.63) is derived on the basis of the electromagnetic equivalence theorem (Schelkunoff, 1943). Thus, the geometric ray-tracing technique can be used to compute the near field on the particle's surface, which can be subsequently mapped to the far field on the basis of eq. (2.63). The mapping idea within the framework of the ray-tracing computation was first employed by Muinonen

(1989) who developed an algorithm known as the modified Kirchhoff approximation (MKA) to solve the scattering by nonspherical ice crystals based on an electromagnetic equation similar to eq. (2.63). To simplify numerical computations, a constant extinction efficiency of 2 was assumed in the MKA and the strong forward-scattering maximum was approximated by the Fraunhofer diffraction. Yang and Liou (1995, 1996b) considered the phase interference and the polarization state of the rays in the near-field computation (hereafter, this method is referred to as GOM2). In GOM2, the extinction cross-section is computed from the fundamental extinction formula (van de Hulst, 1957) or the so-called optical theorem (Bohren and Huffman, 1983) given by

$$\sigma_{\rm ext} = \frac{2\pi}{k^2} \,{\rm Re}\left[A_{\parallel}(\hat{e}_0^{\rm i}) + A_{\perp}(\hat{e}_0^{\rm i})\right], \tag{2.64}$$

where $k = 2\pi/\lambda$ in which λ the incident wavelength. $A_{\parallel}(\hat{e}_0^{\rm i})$ and $A_{\perp}(\hat{e}_0^{\rm i})$ are the amplitude scattering matrix elements in the forward scattering direction for parallel and perpendicular polarization configurations, respectively. In eq. (2.64), the symbol, Re, denotes the real part of the associated quantity. In GOM2, the absorption cross-section of an ice crystal is computed via a rigorous electromagnetic relation (Hage *et al.*, 1991) given by

$$\sigma_{\rm abs} = \frac{k\varepsilon_{\rm i}}{|\boldsymbol{E}^{\rm i}|^2} \iiint_v \boldsymbol{E}(\boldsymbol{r}) \cdot \boldsymbol{E}^*(\boldsymbol{r}\,{\rm d}\boldsymbol{r}, \tag{2.65}$$

where $\varepsilon_{\rm i}$ is the imaginary part of the permittivity, $\boldsymbol{E}^{\rm i}$ is the incident electric vector, and the integration is carried out for the volume of the particle. When eq. (2.65) is applied to the ray-tracing computation, a semi-analytical expression can be derived for the absorption cross-section, as shown by Yang and Liou (1996b).

Similar to the case in eq. (2.63), the far field can be computed if the internal electric field within the scattering particle is known, as is given by the following electrodynamic relation (Saxon, 1973; Goedecke and O'Brien, 1988; Mishchenko *et al.*, 2002):

$$\boldsymbol{E}^{\rm s}(\boldsymbol{r})\big|_{kr\to\infty} = \frac{k^2\,{\rm e}^{ikr}}{4\pi r}(\varepsilon - 1) \iiint_v \{\boldsymbol{E}(\boldsymbol{r}') - \hat{r}[\hat{r}\cdot\boldsymbol{E}(\boldsymbol{r}')]\}\,{\rm e}^{-ik\hat{r}\cdot\boldsymbol{r}'}\,{\rm d}^3r', \tag{2.66}$$

where ε is the permittivity. The advantage of using eq. (2.66) is that only the electric field is involved, whereas both electric and magnetic fields are included in eq. (2.64). In the limit of geometric optics, the incident wave consists of a bundle of rays each of which propagates along a rectilinear path determined by Snell's law. With this assumption, the volume integration in eq. (2.66) can be carried out along the ray paths, and at the same time a semi-analytical solution for the far-field can be derived (Yang and Liou, 1997). This method is referred to as the ray-by-ray integration (RBRI) method in the authors' previous work. Yang and Liou (1997) also showed that RBRI reduces to the anomalous diffraction approximation (ADA) developed by van de Hulst (1957) when the scattering particle is optically tenuous (i.e., the refractive index is close to 1).

The GOM2 and RBRI methods are essentially the same within the context that a hybrid algorithm based on the principles of geometric optics and the near-to-far-field electromagnetic wave theory are employed to compute the single-scattering properties of an ice crystal.

2.3 The finite-Difference Time Domain Method

For size parameters less than about 20–40, the geometric optics method breaks down (Yang and Liou, 1995; 1996b; Macke *et al.*, 1995; Mishchenko and Macke, 1999). Although various methods (see Mishchenko *et al.* 2000) have been developed to solve for the single-scattering properties of nonspherical particles, the finite-difference time-domain (FDTD) method pioneered by Yee (1966) is quite attractive for the computation of light scattering and absorption by small nonspherical and inhomogeneous ice crystals. The FDTD method has been known to be a flexible and robust approach for solving various electromagnetic problems. Publications related to the FDTD method in the literature surveyed by Shlager and Schneider (1998) illustrate the popularity of this method. In particular, several books have been entirely devoted to this particular numerical technique for various applications, ranging from the signal propagation in circuits to the study of the electromagnetic hazard in bioscience (Kunz and Luebbers, 1993; Taflove, 1995; Taflove and Hagness, 2000).

The FDTD method can be technically considered as a 'brute force' approach to solve the time-dependent Maxwell curl equations. Unlike the conventional approach of solving Maxwell's equations in the frequency domain in which an electromagnetic scattering process is posed as a boundary-value problem, the FDTD method solves an electromagnetic problem as an initial-value problem. Mathematically, a boundary-value problem is normally more difficult than its initial-value counterpart. To illustrate the basic concept of the FDTD method for those who do not have any experience on this numerical technique, here we first recapture the FDTD solution for the propagation of a plane electromagnetic wave in free space, which is a typical 1-D wave-propagation problem. Then, we outline the other major numerical aspects (namely, the absorbing boundary condition, the transform of the field from the time domain to the frequency domain, and the mapping of the near field to the far field) involved in the implementation of the FDTD technique for computing the scattering properties of dielectric particles. A comprehensive discussion on the 1-D scalar wave equation in the framework of the finite-difference technique has been presented by Umashankar and Taflove (1982), Taflove (1995) and Taflove and Hagness (2000) who also discussed the 1-D electromagnetic wave propagation for the implementation of the incident wave condition in the FDTD numerical computation.

As shown in Fig. 2.3, a wave propagates along the z-axis of a Cartesian coordinate system. The electric and magnetic vectors associated with this wave are specified along the x- and y-axis of the coordinate system. This is a typical 1-D wave propagation problem and the governing equations for the electromagnetic wave can be written as follows:

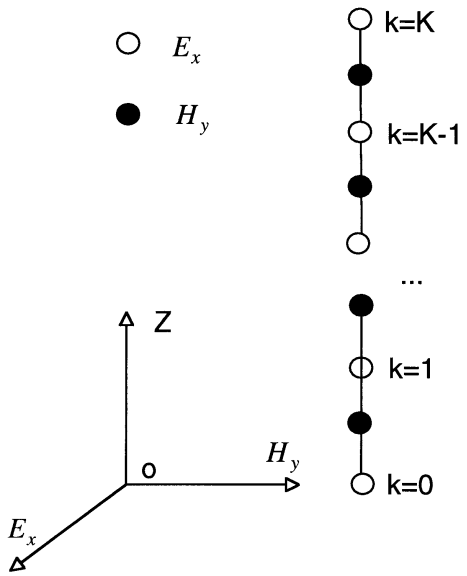

Fig. 2.3. The grid for the one-dimensional finite-difference analog of Maxwell's equations. The propagation of a plane electromagnetic wave is defined as propagating along the z-axis of the coordinate system. The electric and magnetic fields are specified in a staggered manner, i.e., E_x is defined at grid points $k = 0, 1, 2, \ldots, K$ whereas H_y specified at grid points $k = 1/2, 3/2, \ldots, k - 1/2$.

$$\frac{1}{c}\frac{\partial E_x(z,t)}{\partial t} = -\frac{\partial H_y(z,t)}{\partial z}, \tag{2.67}$$

$$-\frac{1}{c}\frac{\partial H_y(z,t)}{\partial t} = \frac{\partial E_x(z,t)}{\partial z}, \tag{2.68}$$

where c is the speed of light in vacuum. To solve variation in the electromagnetic wave, the finite-difference technique is used in the FDTD method, i.e., both electric and magnetic fields are specified in terms of their discrete values in time and space. Following Yee (1966) and Taflove (1995), we define the discrete values of the fields as follows:

$$E^n_{x,k} = E_x(k\,\Delta z,\ n\,\Delta t), \tag{2.69}$$

$$H^{n+1/2}_{y,k+1/2} = H_y\left[(k+1/2)\,\Delta z,\ (n+1/2)\,\Delta t\right], \tag{2.70}$$

where Δz and Δt are the grid size and time increment, respectively, and the indices k and n are integers. The electric and magnetic fields are defined on a stagger grid, i.e., the electric field is specified at grid points with integer indices ($k = 0, 1, 2, \ldots$), whereas the magnetic field is defined at the middle points of adjacent grid points. Similarly, the electric field is defined at time steps $n\,\Delta t$, whereas the magnetic field is defined at time steps $(n+1/2)\,\Delta t$. Using the discrete values of the fields defined in eqs (2.69) and (2.70), the derivatives of the electric and magnetic fields in Maxwell's equations can be expressed in terms of the

standard 'leapfrog' or central difference scheme as follows (Yee, 1966; Taflove, 1995):

$$\left.\frac{\partial E_x(z,t)}{\partial t}\right|_{\substack{z=k\Delta z\\ t=(n+1/2)\Delta t}} \approx \frac{E_x[k\,\Delta z,\ (n+1)\,\Delta t] - E_x[k\,\Delta z,\ n\,\Delta t]}{\Delta t} = \frac{E_{x,k}^{n+1} - E_{x,k}^{n}}{\Delta t}, \tag{2.71}$$

$$\left.\frac{\partial H_y(z,t)}{\partial z}\right|_{\substack{z=k\Delta z\\ t=(n+1/2)\Delta t}} \approx \frac{H_y[(k+1/2)\,\Delta z,\ (n+1/2)\,\Delta t] - H_y[(k-1/2)\,\Delta z,\ (n+1/2)\,\Delta t]}{\Delta z} = \frac{H_{y,k+1/2}^{n+1/2} - H_{y,k-1/2}^{n+1/2}}{\Delta z}, \tag{2.72}$$

Upon substitution of eqs (2.71) and (2.72) into eq. (2.67), the finite-difference analog of eq. (2.67) is given by

$$E_{x,k}^{n+1} = E_{x,k}^{n} + \frac{c\,\Delta t}{\Delta z}\left[H_{y,k-1/2}^{n+1/2} - H_{y,k+1/2}^{n+1/2}\right]. \tag{2.73}$$

Similarly, we can derive the finite difference analog of eq. (2.68) as follows:

$$H_{y,k+1/2}^{n+1/2} = H_{y,k+1/2}^{n-1/2} + \frac{c\,\Delta t}{\Delta z}\left[E_{x,k}^{n} - E_{x,k+1}^{n}\right]. \tag{2.74}$$

The selection of the time increment Δt in the finite analog of Maxwell's equations is not arbitrary because of the stability condition required by the difference equations in numerical computation (Yee, 1966; Taflove and Brodwin, 1975). In the case for 1-D electromagnetic wave, the stability condition requires that $c\,\Delta t/\Delta z \leq 1$.

Equations (2.73) and (2.74) constitute the difference equations for computing variation in the fields. In practice, if the initial values of the fields, say, $E_{x,k}^{1}$ and $H_{y,k+1/2}^{1/2}$ are defined at grid points indicated by indices 0, 1, 2, ... and 1/2, 3/2, 5/2, ..., respectively, this variation can be simulated by a time-marching iteration based on eqs (2.73) and (2.74). However, the computational domain in the numerical simulation must be truncated. For the 1-D case, let the computational domain be the spatial regime bounded by grid point $k = 0$ and $k = K$. From eqs (2.73) and (2.74), the electric fields at $k = 0$ and $k = K$ cannot be computed by these two finite difference equations because $H_{y,-1/2}^{1/2}$ and $H_{y,K+1/2}^{1/2}$ are defined at the locations outside the computational domain. Thus, to update the electric fields at the boundary points, appropriate boundary conditions must be provided. For simplicity in calculating the field values at the boundary grid points, the grid configuration can be specified as follows:

$$c\,\Delta t/\Delta z = 1/2. \tag{2.75}$$

The preceding relation implies that the wave propagates half grid size every time step. Thus, the equations for updating the boundary values can be written as follows:

$$E^n_{x,1/2} = E^{n-1}_{x,1}, \tag{2.76}$$

$$E^{n+1}_{x,0} = E^n_{x,1/2}, \tag{2.77}$$

$$E^n_{x,K-1/2} = E^{n-1}_{x,K-1}, \tag{2.78}$$

$$E^{n+1}_{x,K} = E^n_{x,K-1/2}, \tag{2.79}$$

where $E^n_{x,1/2}$ and $E^n_{x,K-1/2}$ are two auxiliary quantities introduced for updating the electric fields at the two boundary points, respectively. Equations (2.76) and (2.77) constitute the boundary condition for the grid point for $k = 0$, whereas eqs (2.78) and (2.79) constitute the boundary condition for the grid point of $k = K$. Using the finite difference equations (2.73) and (2.74) and the boundary conditions given by eqs (2.76)–(2.79), one can compute variation in the electromagnetic fields within the region between $k = 0$ and K. The computed electromagnetic fields are the same as those in the case where the computational domain is not bounded. Note that if $E^n_{x,0} = 0$ and $E^n_{x,K} = 0$, the boundary grid points constitute the reflecting boundaries. In this case, the electromagnetic wave, when impinges on the boundary grid points, is reflected back to the computational domain and contaminate the numerical simulation. The preceding 1-D finite-difference equations and the associated boundary conditions have been employed to implement the incident wave conditions in various applications of the FDTD technique (e.g., Sullivan *et al.*, 1988).

The discretization of Maxwell's equations in the 3-D case is similar to that in 1-D case. For example, the Maxwell curl equations in the scalar component form for E_x and H_x can be written as follows:

$$\frac{\partial E_x(\boldsymbol{r},t)}{\partial t} = \frac{c}{\varepsilon}\left(\frac{\partial H_z(\boldsymbol{r},t)}{\partial y} - \frac{\partial H_y(\boldsymbol{r},t)}{\partial z}\right), \tag{2.80}$$

$$\frac{\partial H_x(\boldsymbol{r},t)}{\partial t} = -c\left(\frac{\partial E_z(\boldsymbol{r},t)}{\partial y} - \frac{\partial E_y(\boldsymbol{r},t)}{\partial z}\right). \tag{2.81}$$

For simplicity in this discussion, we assume that the permittivity is a real number. Using the standard definitions for the electric and magnetic fields on a grid cell shown in Fig. 2.4 (Yee, 1966), it is straightforward to derive the difference analog of eqs (2.81) and (2.82) on the basis of the central-difference scheme in both time and space as follows:

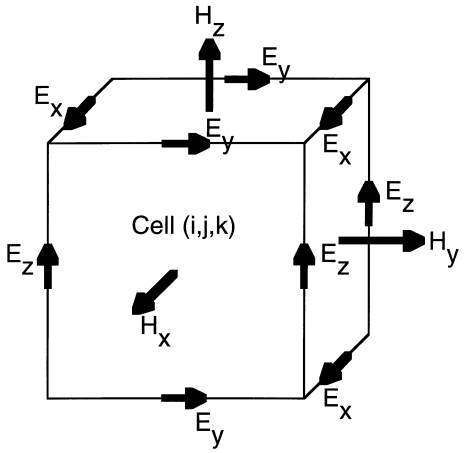

Fig. 2.4. Locations of the electric and magnetic field components on a cubic grid cell, defined by Yee (1966).

$$
\begin{aligned}
E^{n+1}_{x,i,j+1/2,k+1/2} &= E^{n}_{x,i,j+1/2,k+1/2} \\
&\quad + \frac{1}{\varepsilon_{i,j+1/2,k+1/2}} \left[\frac{c\,\Delta t}{\Delta y} (H^{n+1/2}_{z,i,j+1,k+1/2} - H^{n+1/2}_{z,i,j,k+1/2}) \right. \\
&\quad \left. + \frac{c\,\Delta t}{\Delta z} (H^{n+1/2}_{y,i,j+1/2,k} - H^{n+1/2}_{y,i,j+1/2,k+1}) \right], \qquad (2.82)
\end{aligned}
$$

$$
\begin{aligned}
H^{n+1/2}_{x,i+1/2,j,k} &= H^{n-1/2}_{x,i+1/2,j,k} + \left[\frac{c\,\Delta t}{\Delta y} (E^{n}_{z,i+1/2,j-1/2,k} - E^{n}_{z,i+1/2,j+1/2,k}) \right. \\
&\quad \left. + \frac{c\,\Delta t}{\Delta z} (E^{n}_{y,i+1/2,j,k+1/2} - E^{n}_{y,i+1/2,j,k-1/2}) \right]. \qquad (2.83)
\end{aligned}
$$

The finite-difference equations for other components of the electric and magnetic fields can be determined in similar forms. In the 3-D case, the stability condition has been derived by Taflove and Brodwin (1975) given by

$$
c\,\Delta t \leq \frac{1}{\sqrt{1/\Delta x^2 + 1/\Delta y^2 + 1/\Delta z^2}}. \qquad (2.84)
$$

In the 3-D case, the boundary condition is a major issue in the FDTD computation because the analytical boundary equations cannot be constructed due to the unknown propagating directions of the outgoing waves. In the past two decades, various numerical techniques (Blaschak and Kriegsmann, 1988; Moore *et al.*, 1988; Berntsen and Hornsleth, 1994) have been developed to update the field values at the boundary grid points. The commonly used approaches are the absorbing boundary condition developed by Mur (1981), the transmitting boundary condition developed by Liao *et al.* (1984), and the perfectly matched layer (PML) boundary condition pioneered by Berenger (1994, 1996). The PML

is particularly efficient and popular in the implementation of the FDTD numerical scheme (e.g., Katz *et al.* 1994). In the following we briefly outline the principle of the PML boundary condition.

The essence of PML is to introduce an artificial absorbing medium within the boundary layers that impose absorption on the partial electromagnetic field components. For implementing the PML absorbing boundary condition, a field component needs to be split into two parts in the forms

$$(E_x, E_y, E_z) = [(E_{xy} + E_{xz}),\ (E_{yx} + E_{yz}),\ (E_{zx} + E_{zy})], \tag{2.85}$$

$$(H_x, H_y, H_z) = [(H_{xy} + E_{xz}),\ (H_{yx} + H_{yz}),\ (H_{zx} + H_{zy})]. \tag{2.86}$$

The PML boundary condition equations for E_z and H_z components at a boundary perpendicular to the x-axis are given by

$$\frac{\exp[-\tau_x(x)t]}{c}\frac{\partial}{\partial t}\{\exp[\tau_x(x)t]E_{zx}\} = \frac{\partial(H_{yx} + H_{yy})}{\partial x}, \tag{2.87}$$

$$\frac{1}{c}\frac{\partial E_{zy}}{\partial t} = -\frac{\partial(H_{xy} + H_{xz})}{\partial y}, \tag{2.88}$$

$$\frac{\exp[-\tau_x(x)t]}{c}\frac{\partial}{\partial t}\{\exp[\tau_x(x)t]H_{zx}\} = -\frac{\partial(E_{yx} + E_{yz})}{\partial x}, \tag{2.89}$$

$$\frac{1}{c}\frac{\partial H_{zy}}{\partial t} = \frac{\partial(E_{xy} + E_{xz})}{\partial z}, \tag{2.90}$$

where $\tau_x(x)$ is defined for the boundary layers near $x = 0$ as follows:

$$\tau_x(x) = \tau_{\max}|(x - \delta x)/\delta x|^p, \tag{2.91}$$

where $\tau_{\max}$ denotes the maximum absorption at $x = 0$, which can be determined by specifying the reflectance of the boundary layers at a normal incidence. In eq. (2.91), δx denotes the thickness of the boundary layer and p is usually selected between 2 and 3 (Lazzi and Gandi, 1996). In numerical computations, the PML boundary condition is applied to outgoing scattered waves. To do so, the FDTD computational is usually divided into an inner domain enclosed by an outer domain. Within the inner domain, the total field (incident plus scattered fields) is simulated, and only outgoing or scattered field is simulated otherwise. In practice, an interface known as the Huygens surface (Merewether *et al.*, 1980) is introduced to connect the fields in the two domains. Note that, to avoid the Huygens surface, an alternative approach for which the scattered field is defined for the entire computational domain has been developed (e.g., Britt, 1989; Yang and Liou, 1995). However, this approach is not computationally efficient, particularly, for the implementation of the FDTD method in the 3-D case.

With the finite difference analog of the Maxwell equations and the absorbing boundary condition, the electromagnetic field within or near a scattering particle (i.e., the near field) in the time domain can be obtained. The corresponding signal in the frequency domain can be obtained via the discrete Fourier transform. For example, if the time series of electric field at a given grid point say,

$E^{n+1}_{x,i,j+1/2,k+1/2}$, are known, the corresponding signal in the frequency domain can be obtained as follows

$$E_{x,i,j+1/2,k+1/2}(k) = \sum_{n=0}^{N} E^{n+1}_{x,i,j+1/2,k+1/2} \exp(i2\pi cn\,\Delta t/\lambda), \tag{2.92}$$

The discrete Fourier transform is more efficient than the fast Fourier transform for application to the FDTD computation, as illustrated by Furse and Gandhi (1995).

After the near field in the frequency domain is obtained, the scattered far field can be obtained from either eq. (2.63) or eq. (2.66). Although these two equations are physically equivalent, the far-field values computed from eqs (2.63) and (2.66) differ in terms of accuracy (Zhai *et al.*, 2004). The near-to-far-field transformation in both the frequency and time domains has been discussed by Taflove and Hagness (2000) and references cited therein.

2.4 Numerical Examples

The FDTD technique has been applied to the investigation of the scattering properties of small ice crystals (Yang and Liou, 1995, 1996a; Sun *et al.*, 1999; Sun and Fu, 2000; Yang *et al.*, 2004a) and its accuracy has been extensively studied in reference to the results computed from the 'exact' Lorenz–Mie theory for spheres. Also, Baran *et al.* (2001) compared the FDTD solution and T-matrix results for the single-scattering properties of hexagonal ice crystals. In general, the relative errors of the FDTD solutions are typically less than 1% for computing the extinction and absorption cross-sections and on the order of 10% for computing the phase function if the grid size is less than 1/20 of the wavelength within the scattering particle of interest. The accuracy of the FDTD solution can be further improved if a finer grid size is used, but at the expense of the computational CPU time. In practice, application of the FDTD technique to the light scattering by ice crystals is limited to size parameters less than about 20 because enormous computational efforts are required. Sun *et al.* (1999) applied this method to the solution to the scattering of light by a single ice sphere with a size parameter of 40 at a wavelength at which the refractive index of ice is small. Application of the FDTD technique to the scattering of light by particles with a large refractive index (e.g., the real part of the refractive index is on the order of 8) has been recently reported by Sun and Fu (2000) and Yang *et al.* (2004a). The latter authors also applied this method to complex bullet rosette ice crystals with various branches (Yang *et al.*, 2004a). As an example, Fig. 2.5 shows comparison of the phase matrix elements computed from the FDTD technique and the Lorenz–Mie theory for an ice sphere with a size parameter of 20 at a wavelength of 0.6328 μm. A surface-integral based approach (Zhai *et al.*, 2004) with a grid resolution of $\lambda/\Delta s = 40$ is used to map the near field to far field for the FDTD resolute shown in Fig. 2.5, where λ and Δs are the incident wavelength and grid size, respectively. Excellent agreement between the FDTD

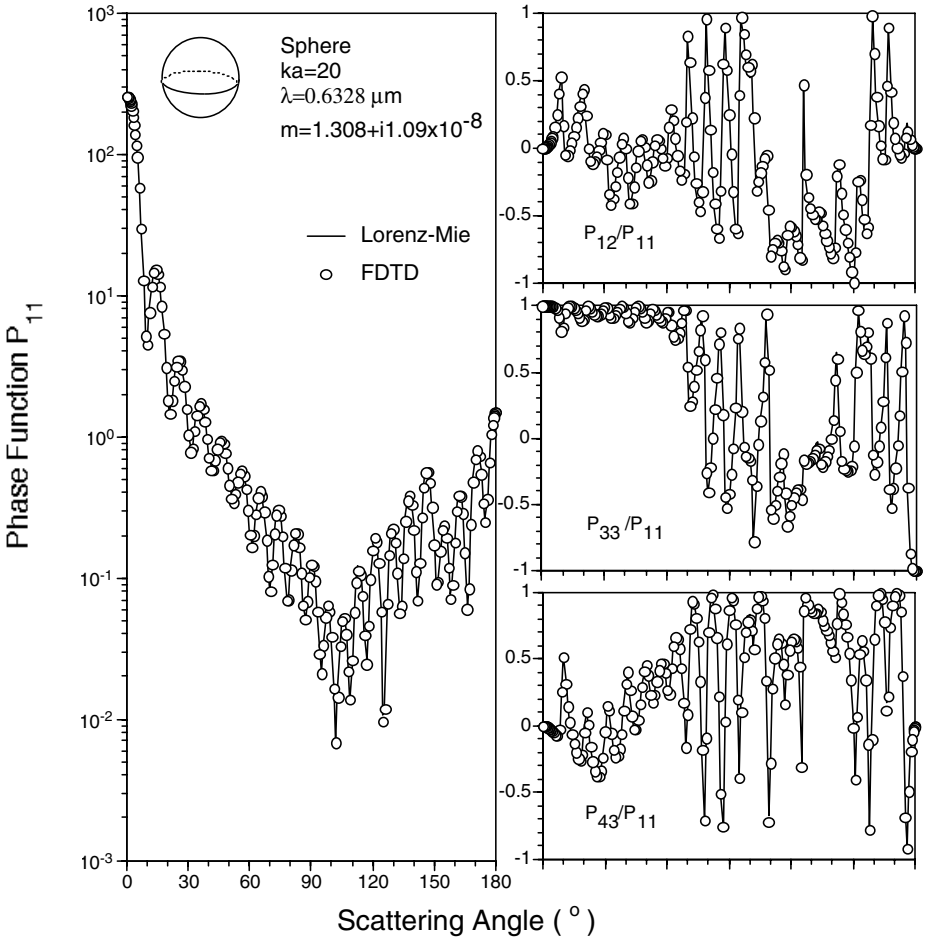

Fig. 2.5. Comparison of the phase matrix elements computed from the Lorenz–Mie theory and the FDTD method for an ice sphere with a size parameter of 20 using a wavelength of 0.6328 μm.

and Lorenz–Mie results is evident. The FDTD solution for the phase function is more accurate than for the other phase matrix elements because former is less sensitive to phase variation in the scattered waves.

It has been commonly assumed that a small quasi-spherical ice crystal may be approximated by an equivalent sphere, defined by (1) the same diameter (D), (2) the same surface area (A), (3) the same volume (V), or (4) the same ratio of V to A. Fig. 2.6 shows comparison of the phase functions computed for these four definitions of spherical equivalence for Platonic solids (i.e., tetrahedron, hexahedron, octahedron, dodecahedron, and icosahedron). It is interesting to note that the study of the Platonic-solid shape has a rich history, which goes back to the beginning of recorded human civilization. For example,

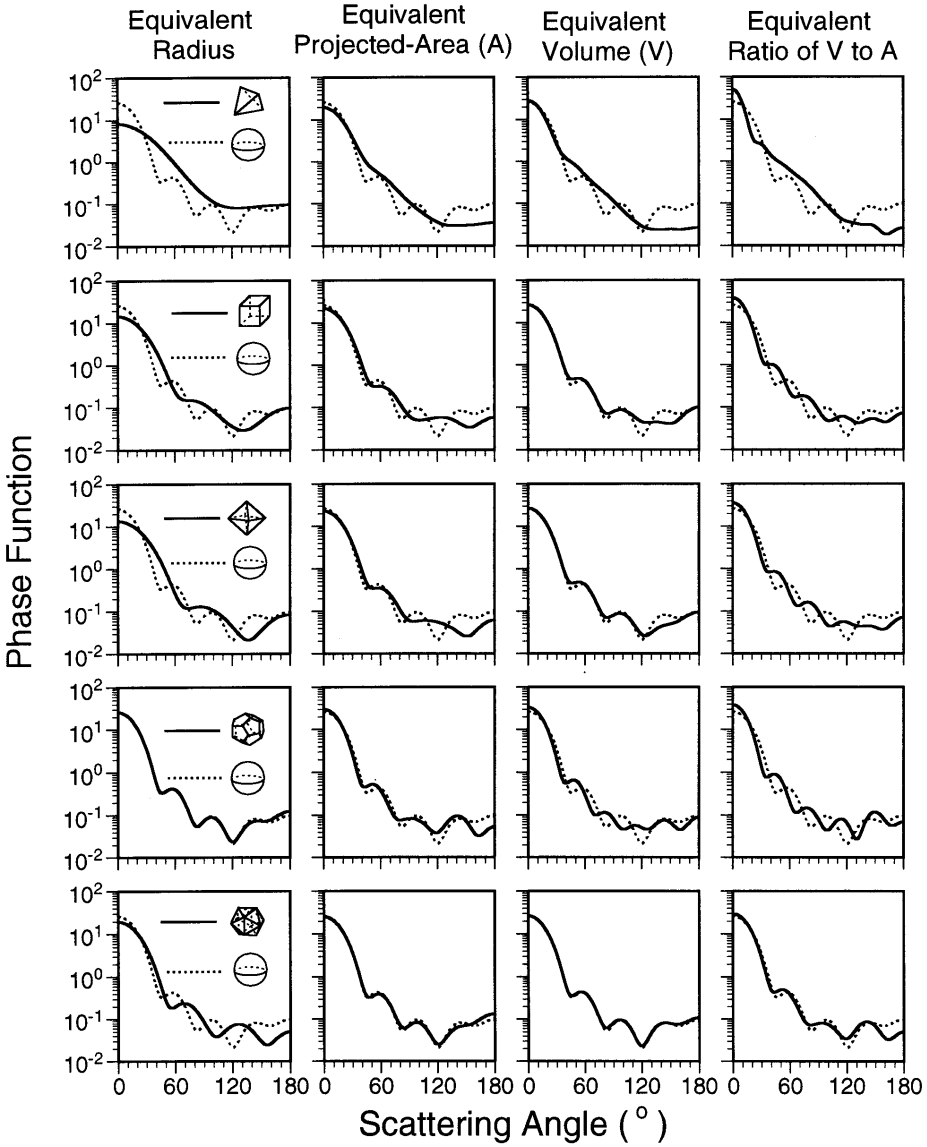

Fig. 2.6. The phase function of an ice sphere with a size parameter of $x = 5$. The wavelength and refractive index are 0.6328 μm and $1.3085 + \mathrm{i}1.09 \times 10^{-8}$, respectively. Also shown are the phase functions of the five Platonic shapes with the same radius (the first column), projected area (the second column), volume (the third column) and V/A (the fourth column) as those for the ice sphere (after Yang *et al.*, 2004b).

the polyhedron was extensively used/investigated in ancient Egyptian, Babylonian, Chinese, and Greek cultures associated with the study of architecture, art, mathematics, and even the philosophy regarding the early understanding

of the universe. Historically, it was believed that matter was composed of a few elemental substances combined in different ways. Influenced by Aristotle (384–322 **BC**), ancient wisdom assumed that the basic elements (fire, air, earth, water, and celestial matter) were related to the five regular polyhedra. A review of the history of the study of polyhedron can be found in a monograph by Cromwell (l997) and also in a review article by Field (1979). Although the polyhedron has been studied for millennia from various perspectives, it is still a challenging topic for modern mathematicians. In fact, many mathematical theorems related to the polyhedron have only recently been proved (e.g., Grunbaum, 1967). The numbers of the faces for a tetrahedron, a cube, an octahedron, a dodecahedron, and an icosahedron are 4, 6, 8, 12, and 20, respectively. The faces of a Platonic solid are equilateral polygons with the same number of sides. The number of faces, the number of vertices, and the number of edges of a polyhedron satisfy the famous Euler's theorem (Euler, 1758) that can be expressed as follows:

$$f + v + e = 2, \tag{2.93}$$

where f is the number of polygon faces, v the number of vertices, and e the number of edges. The five platonic solids approach spheres in an orderly manner and, therefore, they are ideal for investigating the asphericity effect on the scattering properties. It is evident from Fig. 2.6 that a systematically optimized definition for 'spherical equivalence' does not exist. It is seen that the 'spherical equivalence' based on the particle dimension leads to the best approximation in the case for dodecahedron, whereas the volume-based 'equivalence' is more accurate than the other three definitions in the case of the icosahedron. It is clear that the extent of nonsphericity of a particle in the context of light scattering computation depends on a specific geometry. This implies that a general optimal 'spherical equivalence' cannot be defined to minimize the errors associated with the spherical approximation for a variety of nonspherical geometries in light scattering computations.

The simplest ice crystal shape can be represented by the pristine column and plate that normally have a basic hexagonal symmetric structure. Using the geometric ray-tracing technique, the scattering properties of hexagonal ice crystals have been extensively investigated in the past. The pristine ice crystal types produce the well-known 22° and 46° halos, as well as a number of fascinating arcs and sundogs that have been observed in cirrus cloud conditions (see for example, Greenler, 1990).

The upper panels of Fig. 2.7 show the nonzero phase matrix elements for randomly oriented hexagonal ice columns at a wavelength of 0.6328 μm. For the scattering of light by large particles with a size parameter on the order of those shown in Fig. 2.7, the conventional and improved geometric optics methods produce about the same results. The peaks at 22° and 46° scattering angles in the phase function are responsible for the halos observed in the atmosphere. The scattering maximum between 150° and 160° is produced by the rays undergoing two internal reflections (Takano and Liou, 1989a). The lower panels in Fig. 2.7

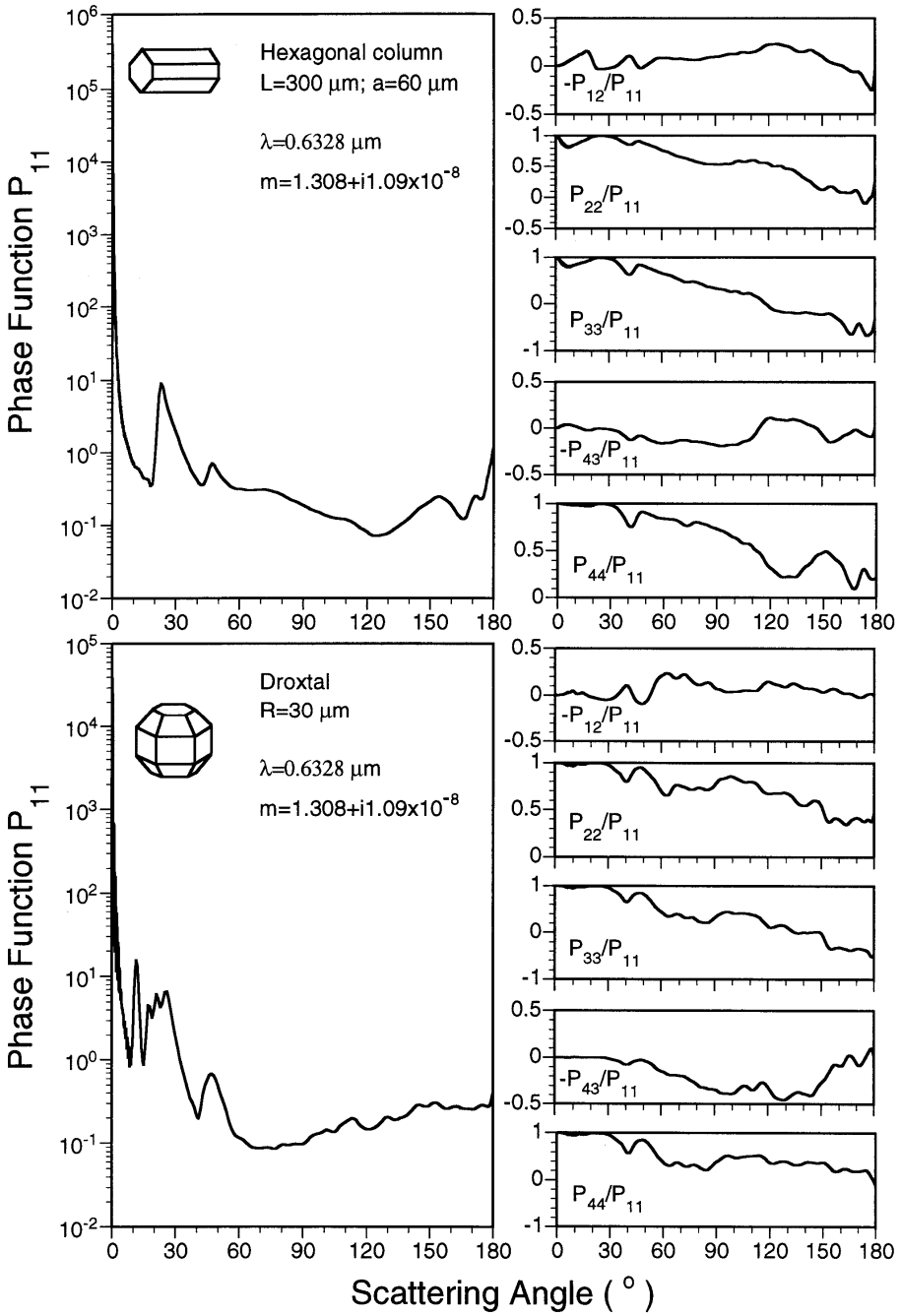

Fig. 2.7. The scattering phase matrix of randomly oriented hexagonal ice columns and droxtal ice crystals computed from the geometric optics method for large size parameters.

show the nonzero phase matrix elements for randomly oriented droxtal, an ice crystal term introduced by Thuman and Robinson (1954) and Ohtake (1970). The droxtal geometry with a 20-face structure has been suggested as a better representation of small quasi-spherical ice crystals observed in ice clouds. It has been speculated that the formation of droxtal ice crystals is associated with the freezing of supercooled water droplets and subsequent growth by water vapor deposition (Zhang *et al.*, 2004). From Fig. 2.7, it is evident that the single-scattering properties of droxtal ice crystals are substantially different from those of well-defined pristine hexagonal ice crystals. For the former, the phase function is quite flat at large scattering angles from 100° to 180°. Additionally, droxtals scatter less energy than hexagonal ice crystals in the scattering directions around 60°. A strong peak at the 11° scattering angle in the phase function of droxtals is produced by rays undergoing two sequential refractions through the trapezoidal and rectangular faces.

Fig. 2.8 illustrates the phase matrix for randomly oriented small hexagonal ice crystals and droxtals computed from FDTD. Based on laboratory and aircraft observations, small ice crystals tend to have unit aspect ratio (Auer and Veal, 1970), i.e., $L/2a \sim 1$ in which L and a are the length and semi-width of an ice crystal, respectively. The pronounced scattering peaks corresponding to halos are not observed in the phase function. However, a scattering maximum is shown for both small hexagons and droxtals that are randomly oriented in space. We also note that the phase function for droxtals shows fluctuations in the side and backscattering directions, which cannot be smoothed out through random orientation averaging. Although the overall geometry of a droxtal is close to a sphere, significant nonsphericity effect is noted from the phase matrix. For a sphere, the ratio P_{22}/P_{11} is one. It has been argued that the deviation of P_{22}/P_{11} from unity is an index of nonsphericity effect (Bohren and Huffman, 1983; Mishchenko *et al.* 2002). From Fig. 2.8, the P_{22}/P_{11} values for droxtals for the scattering angles larger than 60° are substantially deviated from unity, indicating the prominent nonspherecity effect. Yang *et al.* (2003) and Zhang *et al.* (2004) have proposed that small quasi-spherical ice crystals in ice clouds may be approximated as droxtals in light scattering computations.

To compare the single-scattering properties for various ice crystal shapes, Figs. 2.9 and 2.10 show the phase functions for six ice crystal habits with small and large size parameters, respectively. For large aggregates, their surfaces are assumed to be moderately rough in the phase function computation on the basis of the Gram–Charlier distribution (Cox and Munk, 1954) following the method described in Yang and Liou (1998). It is evident from Fig. 9 that the scattering of light by small ice crystals does not produce halo peaks. For small plates and columns (the panels in the second row) the phase functions are smooth for scattering angles from 90° to 180°. On the contrary, the overall feature of the phase function for large ice crystals illustrates pronounced peaks, except in the case of aggregates because surface roughness smooths out the scattering peak.

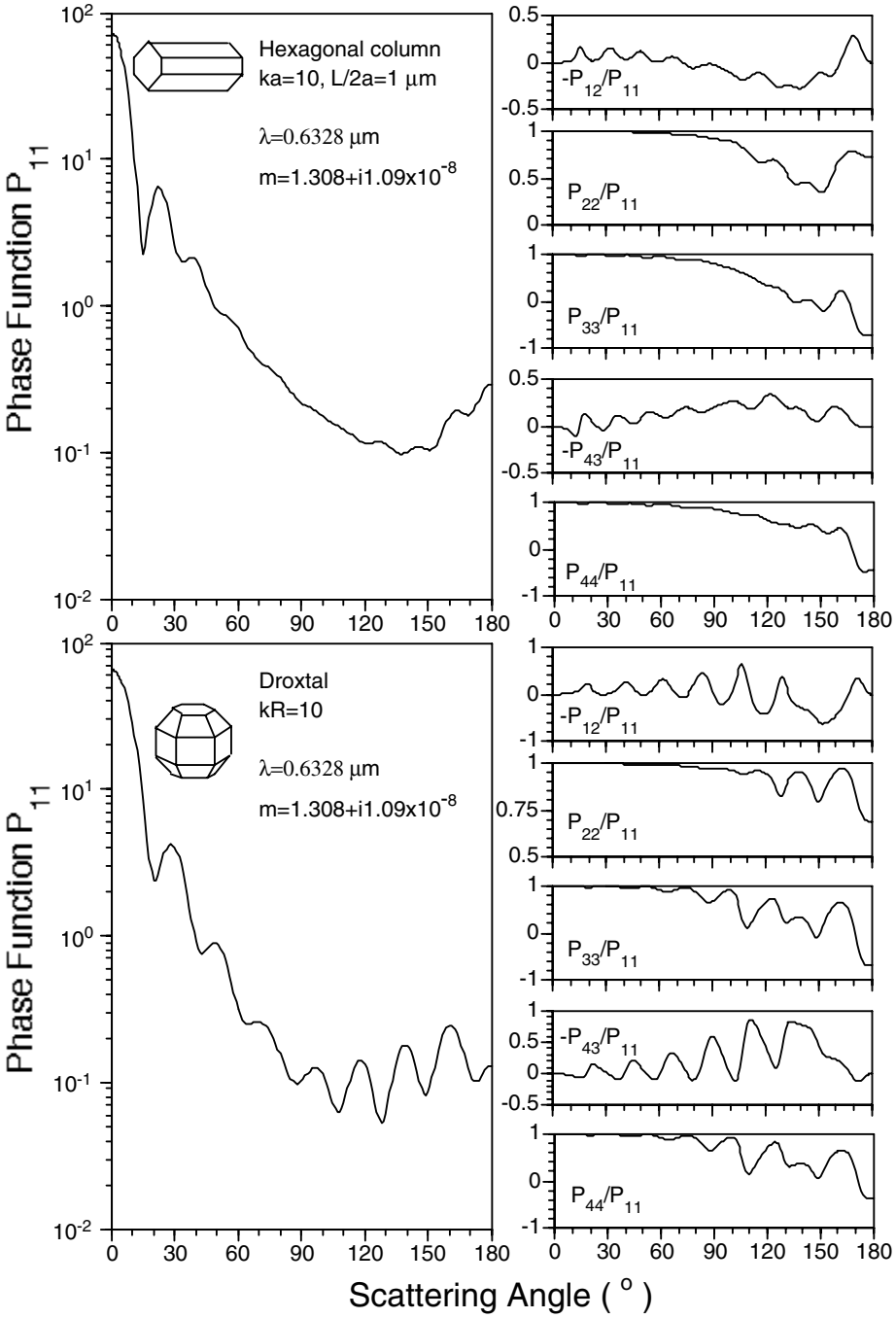

Fig. 2.8. The phase matrix of small compact hexagonal and droxtal ice crystals computed from the FDTD method.

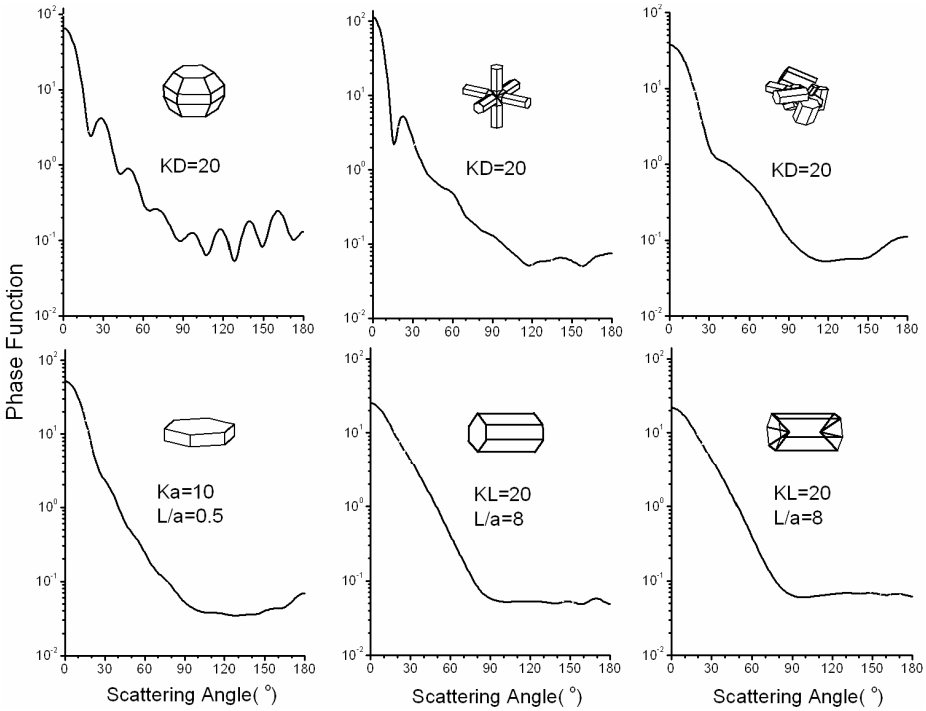

Fig. 2.9. Comparison of the phase functions computed from the FDTD method for ice ice crystal shapes that are commonly observed in ice clouds. The parameter, D, is the maximum dimension for a droxtal, a bullet rosette, or an aggregate ice crystal. For plates and columns, a denotes the half-width and L is the length (for columns) or thickness (for plates). $K = 2\pi/\lambda$ is the wavenumber.

To demonstrate the improvement in GOM2 (Yang and Liou, 1995) as compared to the conventional ray-tracing approach for moderate size parameters, Fig. 2.11 shows the phase function computed by the two methods and FDTD in a 2D case. In the computation, ice crystals were assumed to be infinitely long hexagonal columns with normal incidence. Halo peaks are noticed in the conventional ray-tracing solution, but not in the FDTD result. The scattering patterns produced by the improved geometric optics are similar to those shown in FDTD for both size parameters, but its accuracy is degraded in scattering angles larger than $\sim 100°$.

Fig. 2.12 shows the extinction efficiency and single-scattering albedo computed from FDTD, GOM2 based on eq. (2.63), RBRI based on eq. (2.66), and the conventional ray-tracing technique. The limitation of the conventional ray-tracing method is evident in the evaluation of the extinction efficiency, which is equal to 2 regardless of the size parameter. At a size parameter of about 20, the results computed from RBRI, GOM2, and FDTD converge. Owing to the limitations of the geometric optics approximation and computational requirements

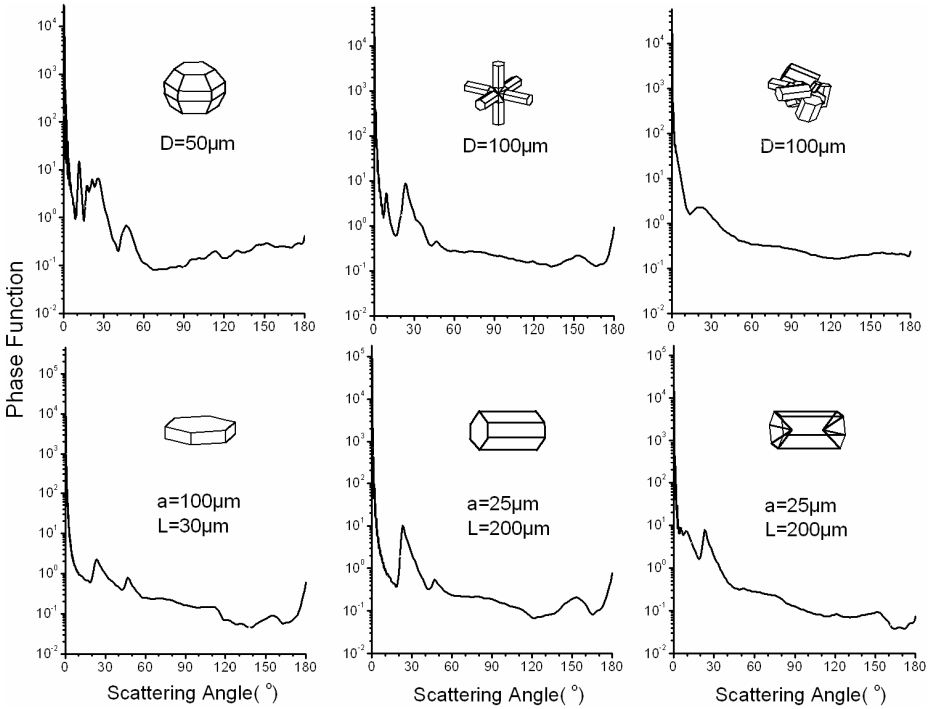

Fig. 2.10. Comparison of the phase functions computed from the geometric optics method for six ice crystal shapes. For aggregates, surface roughness is included in the light scattering computation.

in the FDTD method, they can be applied to large (>20) and small (<20) size parameters, respectively. However, by combining GOM2 and FDTD, calculation of the single-scattering properties for various ice crystal shapes and sizes can be carried out. This is the essence of the unified theory concept developed by Liou *et al.* (2000) in the sense that the accurate FDTD solution can be used for small size parameters and at the same time an approximate geometric optics approach can be applied to large size parameters.

2.5 Summary

In this chapter, we have reviewed the theoretical development and numerical computation for the single-scattering properties of atmospheric ice crystals. Application of two numerical methods, the geometric optics approach and the FDTD technique, to the scattering of light by ice crystals have been highlighted. Specifically, we recaptured the ray-tracing methodology originally developed by Cai and Liou (1982), which is systematically formulated in a vector form in the present presentation. The vector formulation of the ray-tracing procedure is independent of specific coordinate systems and can be implemented in numerical

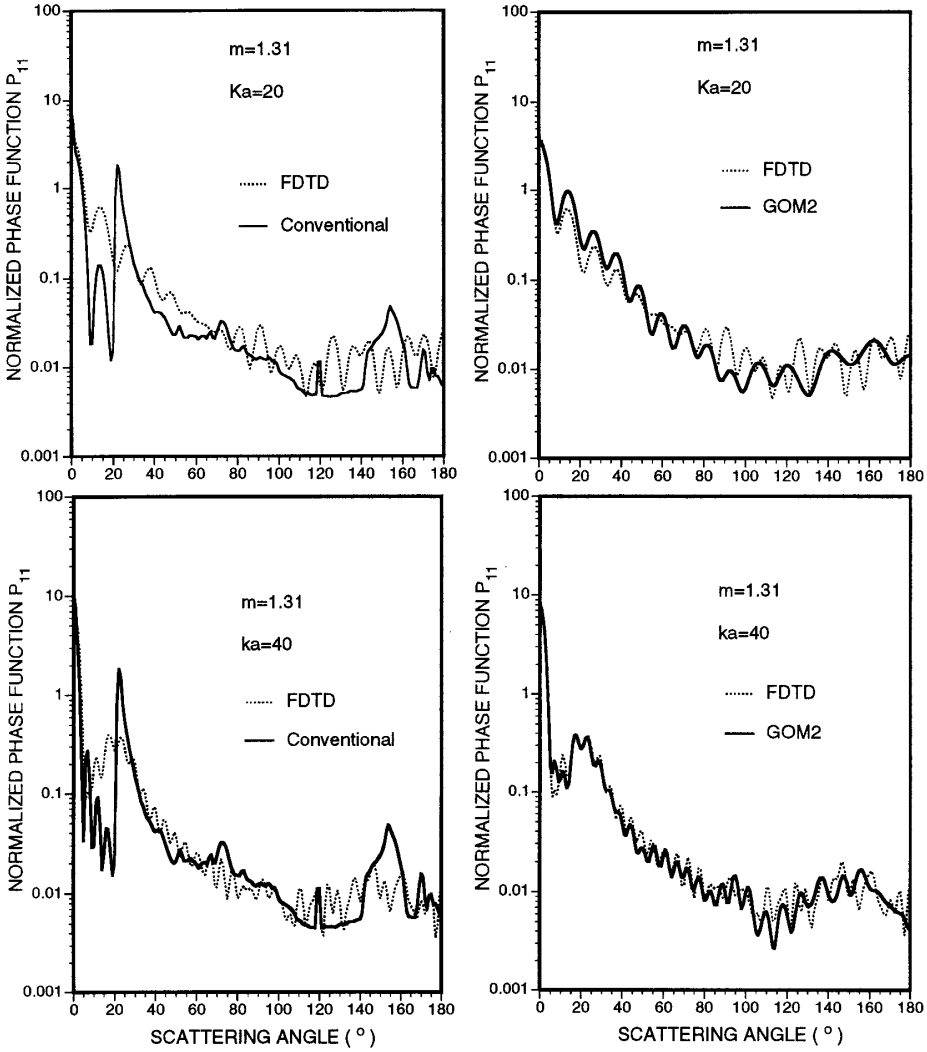

Fig. 2.11. Normalized phase functions computed by the FDTD, conventional ray-tracing, and GOM2 methods for the scattering of light by randomly oriented 2-D hexagonal ice crystals (after Yang and Liou, 1995).

computations effectively. The weightings of diffraction, Fresnel refraction and reflection, and the delta-transmission have been explicitly given in the formulation of the phase matrix. Moreover, the absorption cross-section of ice crystals under the randomly oriented condition is also presented within the framework of the geometric optics approach in which both polarization configurations are accounted for.

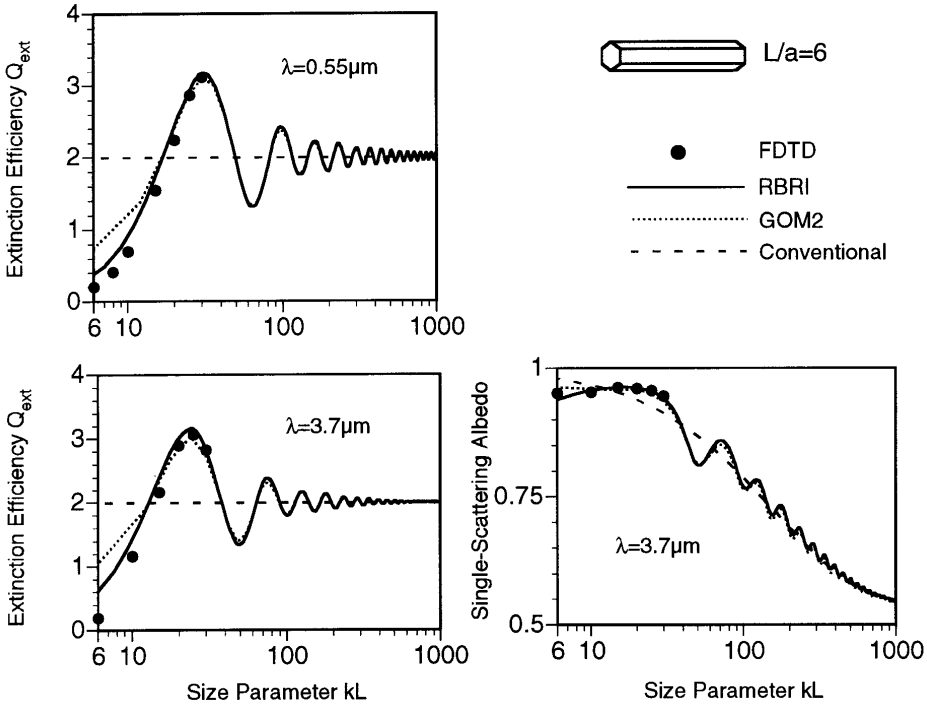

Fig. 2.12. Comparison of the extinction efficiency and the single-scattering albedo computed by FDTD, RBRI, GOM2, and the conventional ray-tracing methods at the 0.55-μm and 3.7-μm wavelengths (data taken from Yang and Liou, 1997).

The FDTD techniques pioneered by Yee (1966) and further developed by many others (e.g., Taflove and Hagness (2000) and references cited therein) is an attractive approach to deal with the scattering of light by small ice crystals. We reviewed the basic principle of the FDTD technique by using the 1-D electromagnetic wave propagation process for illustration. The implementation of FDTD in the 3-D case for the scattering of light by ice crystals was outlined, including the discretization of Maxwell's equations on the basis of the difference approximation, the absorption boundary condition for truncating the computational domain, the transform of simulated signals from the time to the frequency domain, and the near field to far field mapping.

Finally, selected numerical results were presented to illustrate the scattering characteristics of large and small ice crystals. The overall feature for the scattering of light by large ice crystals is that the corresponding phase functions normally show strong halo peaks. However, if the surface roughness condition is imposed in the ray-tracing computation, the scattering peaks associated with halos are largely smoothed out. For small ice crystals, the scattering phase functions are generally featureless in the side and backward scattering directions.

Moreover, we revisited some of our previous numerical results to demonstrate certain advantages of the improved geometric optics methods.

Acknowledgments

The authors thank G. Chen, Z. Zhang and P. Zhai for assisting in numerical computation and graphical presentation. During the course of this research, Ping Yang and K. N. Liou were supported by the National Science Foundation under Grants ATM-458131 and ATM-0331550, respectively. Ping Yang would also like to acknowledge support (NAG5-11374) from the NASA Radiation Sciences Program.

References

Asano, S., and G. Yamamoto, 1975: Light scattering by randomly oriented spheroidal particles, *Appl. Opt.* **14**, 29–49.

Auer, A., and D. Veal, 1970: The dimensions of ice crystals in natural clouds. *J. Atmos. Sci.* **27**, 919–926.

Baran, A. J., P. Yang, and S. Havemann, 2001: Calculation of the single-scattering properties of randomly oriented hexagonal ice columns: a comparison of the T-matrix and the finite-difference time-domain methods, *Appl. Opt.* **40**, 4376–4386.

Berenger, B. J., 1994: A perfectly matched layer for the absorption of electromagnetic waves. *J. Comput. Phys.* **114**, 185–200.

Berenger, B. J., 1996: Three-dimensional perfect matched layer for the absorption of electromagnetic wave. *J. Comput. Phys.* **127**, 363–379.

Berntsen, S., and S. N. Hornsleth, 1994: Retarded time absorbing boundary conditions. IEEE Trans. *Antennas Propagat.* **42**, 1059–1064.

Blaschak, J. G., and G. A. Kriegsmann, 1988: A comparative study of absorbing boundary conditions. *J. Comput. Phys.* **77**, 109–139.

Bohren, C. F., and D. R. Huffman, 1983: *Absorption and Scattering of Light by Small Particles.* John Wiley, New York.

Born, M., and E. Wolf, 1959: *Principles of Optics* (Pergamon, Oxford).

Borovoi, A., I. Grishin, E. Naats, and U. Oppel, 2002: Light backscattering by hexagonal ice crystals. *J. Quant. Spectrosc. Radiat. Transfer* **72**, 403–417.

Borovoi, A. G., and I. A. Grishin, 2003: Scattering matrices for large ice crystal particles. *J. Opt. Soc. Am. A* **20**, 2071–2080.

Britt, C. L., 1989: Solution of electromagnetic scattering problems using time domain techniques. *IEEE Trans. Antennas Propagat.* 37, 1181–1191.

Cai, Q., and K. N. Liou, 1982: Polarized light scattering by hexagonal ice crystals: theory. *Appl. Opt.* **21**, 3569–3580.

Chang, P. C., J. G., Walker, K. I. Hopcraft, 2005: Ray tracing in absorbing media. *J. Quant. Spectrosc. Radiative Transfer* (in press).

Chen, B., and J. J. Stamnes, 1998: Validity of diffraction tomography based on the first born and the first Rytov approximations. *Appl. Opt.* **37**, 2996–3006.

Coleman, R., and K. N. Liou, 1981: Light scattering by hexagonal ice crystals. *J. Atmos. Sci.* **38**, 1260–1271.

Cox, C., and W. Munk, 1954: Measurement of the roughness of the sea surface from photographs of the sun's glitter. *J. Opt. Amer. Soc.* **44**, 838–850.

Cromwell, P. R., 1997: *Polyhedra*. Cambridge University Press, Cambridge, UK.

Dessler, A. E., and P. Yang, 2003: The distribution of tropical thin cirrus clouds inferred from Terra MODIS data. *J. Climate* **16**, 1241–1247.

Dupertuis, M. A., Proctor, M., and B. Acklin, 1994: Generalization of complex Snell–Descartes and Fresnel laws. *J. Opt. Soc. Am. A* **11**, 1159–1166.

Draine, B. T., and P. J. Flatau, 1994: Discrete-dipole approximation for scattering calculations. *J. Opt. Soc. Am. A* **11**, 1491–1499.

Ebert, E. E. and J. A. Curry, 1992: A parameterization of cirrus cloud optical properties for climate models. J. *Geophys. Res.* **97**, 3831–3836.

Euler, L., 1758: Elementa doctrinae solidorum, novi commentarii academiae. *Scientiarum Petropolitanae* **4**, 109–140.

Field, J. V., 1979: Kepler's star polyhedra, *Vistas in Astronomy* **23**, 109–141.

Fu, Q., and K. N. Liou, 1993: Parameterization of the radiative properties of cirrus clouds. *J. Atmos. Sci.* **50**, 2008–2025.

Furse, C. M., and O. P. Gandhi, 1995: Why the DFT is faster than the FFT for FDTD time-to-frequency domain conversions, *IEEE Microwave Guided Wave Lett.* **5**, 326–328.

Gao, B.-C., and Y. J. Kaufman, 1995: Selection of the 1.375-μm MODIS channels for remote sensing of cirrus clouds and stratospheric aerosols from space. *J. Atmos. Sci.* **52**, 4231–4237.

Goedecke, G. H., and S. G. O'Brien, 1988: Scattering by irregular inhomogeneous particles via the digitized Green's function algorithm. *Appl. Opt.* **27**, 2431–2438.

Greenler, R., 1990: *Rainbows, Halos, and Glories.* Cambridge University Press, New York.

Grunbaum, B., 1967: *Convex Polytopes*. John Wiley, London.

Grynko, Y., and Shkuratov, 2003: Scattering matrix calculated in geometrix optics approximation for semitransparent particles faceted with various shapes. *J. Quant. Spectrosc. Radiat. Transfer* **78**, 319–340.

Hage, J. I., J. M. Greenberg, and R. T. Wang, 1991: Scattering from arbitrary shaped particles: theory and experiment. *Appl. Opt.* **30**, 1141–1152.

Heymsfield, A. J., and J. Iaquinta, 2000: Cirrus crystal terminal velocities. *J. Atmos. Sci.* **57**, 916–938.

Hess, M., and Wiegner, M., 1994: COP: a data library of optical properties of hexagonal ice crystals. *Appl. Opt.* **33**, 7740–7746.

Holland, R., 1977: Threde: a free-field EMP coupling and scattering code. *IEEE Trans. Nuclear Science* **24**, 2416–2421.

Holton, J. R., and A. Gettelman, 2001: Horizontal transport and the dehydration of the stratosphere. *Geophys. Res. Lett.* **28**, 2799–2802.

Houze, R. A. Jr, 1993: *Cloud Dynamics*. Academic Press, San Diego, CA.

Iaquinta, J., H. Isaka, and P. Personne, 1995: Scattering phase function of bullet rosette ice crystals, *J. Atmos. Sci.* **52**, 1401–1413.

Jackson, J. D., 1998: *Classical Electrodynamics*, 3rd edn. John Wiley, New York.

Jacobowitz, H., 1971: A method for computing the transfer of solar radiation through clouds of hexagonal ice crystals. *J. Quant. Spectrosc. Radiat. Transfer* **11**, 691–695.

Jensen, E. J., O. B. Toon, L. Pfister, and H. B. Selkirk, 1996: Dehydration of upper troposphere and lower stratosphere by subvisible cirrus clouds near the tropical tropopause. *Geophys. Res. Lett.* **23**, 825–828.

Kahnert, F. M., 2003: Numerical methods in electromagnetic scattering theory. *J. Quant. Spectrosc. Radiat. Transfer* **79–80**, 775–824.

Katz, D. S., E. T. Thiele, and A. Taflove, 1994: Validation and extension to three dimensions of Berenger PML absorbing boundary condition for FD-TD meshes. *IEEE Microwave Guided Wave Lett.* **4**, 268–270.

Kerker, M., 1969: *The Scattering of Light and Other Electromagnetic Radiation*. Academic Press, New York.

King, M. D., W. P. Menzel, Y. J. Kaufman, D. Tanre, B.-C. Gao, S. Platnick, S. A. Ackerman, L. A. Remer, R. Pincus, and P. A. Hubanks, 2003: Cloud and aerosol properties, precipitable water, and profiles of temperature and humidity from MODIS. *IEEE Trans. Geosci. Remote Sensing* **41**, 442–458.

Kokhanovsky, A., 1999: *Optics of Light Scattering Media*. John Wiley, Chichester, UK.

Kress, R. 1990: Nmerical solution of boundary integral equations in time-harmonic electromagnetic scattering. *Electromagnetics* **10**, 1–20.

Kunz, K. S., and L. Simpson, 1981: A technique for increasing the resolution of finite-difference solutions of the Maxwell's equation. *IEEE Trans. Electromagnetic Campat.* **23**, 419-422.

Kunz, K. S., and K. M. Lee, 1978: A three-dimensional finite-difference solution of the external response of an aircraft to a complex transient EM environment, I: The method and its implementation. *IEEE Trans. Electromagnetic Campat.* **20**, 328–333.

Kunz, K. S., and R. J. Luebbers, 1993: *The Finite Difference Time Domain Method for Electromagnetics*. CRC Press, Boca Raton, FL.

Lazzi, G., and O. P. Gandhi, 1996: On the optimal design of the PML absorbing boundary condition for the FDTD code. *IEEE Trans. Antennas Propagat.* **45**, 914–916.

Liao, Z., H. L. Wong, B. Yang, and Y. Yuan, 1984: A transmitting boundary for transient wave analyses. *Scientia Sinica* **XXVII**, 1063–1076.

Liou, K. N., 1972a: Electromagnetic scattering by arbitrarily oriented ice cylinders. *Appl. Opt.* **11**, 667–674.

Liou, K. N., 1972b: Light scattering by ice clouds in the visible and infrared: a theoretical study. *J. Atmos. Sci.* **29**, 524–536.

Liou, K .N., 1973: Transfer of solar irradiance through cirrus cloud layers. *J. Geophys. Res.* **78**, 1409–1418.

Liou, K. N., 1986: Influence of cirrus clouds on weather and climate process: a global perspective. *Mon. Weather Rev.* **114**, 1167–1199.

Liou, K. N. 1992: *Radiation and Cloud Processes in the Atmosphere*. Oxford University Press, New York.

Liou, K. N. 2002: *An Introduction to Atmospheric Radiation*, 2nd edn. Academic Press, San Diego, CA.

Liou, K. N., and J. E. Hansen, 1971: Intensity and polarization for single scattering by polydisperse spheres: a comparison of ray optics and Mie theory. *J. Atmos. Sci.* **28**, 995–1004.

Liou, K. N., and Y. Takano, 2002: Interpretation of cirrus cloud polarization measurements from radiative transfer theory. *Geophys. Res. Lett.* **29**, 10.1029/2001GL014613,27-1-27-4.

Liou, K. N., Y. Takano, and P. Yang, 2000: Light scattering and radiative transfer by ice crystal clouds: applications to climate research, in *Light Scattering by Nonspherical Particles: Theory, Measurements, and Geophysical Applications*, M. I. Mishchenko, J.W. Hovenier, and L. D. Travis (eds), pp. 417–449. Academic Press, San Diego, CA.

Lord Rayleigh, 1918: The dispersal of light by a dielectric cylinder. *Phil. Mag.* **36**, 365–376.

Lorenz, L. V., 1890, Lysbevaege i og uder en plane lysbolger belyst kulge. *Vidensk. Selk. Skr.* **6**, 1–62.

Lynch, D. K., K. Sassen, D. O'C Starr, and G. Stephens (eds), 2002: *Cirrus*. Oxford University Press, New York.

Macke, A., 1993: Scattering of light by polyhedral ice crystals. *Appl. Opt.* **32**, 2780–2788.

Macke, A., M. I. Mishchenko, K. Muinonen, and B. E. Carlson, 1995: Scattering of light by large nonspherical particles: ray-tracing approximation versus T-matrix method. *Opt. Lett.* **20**, 1934–1936.

Macke, A. J. Mueller, and E. Raschke, 1996a: Single scattering properties of atmospheric ice crystal. *J. Atmos. Sci.* **53**, 2813–2825.

Macke, A., M. I. Mishchenko, and B. Cairns, 1996b: The influence of inclusions on light scattering by large ice particles. *J. Geophys. Res.* **101**, 23311–23316.

Macke, A. 2000: Monte Carlo calculations of light scattering by large particles with multiple internal inclusions, in *Light Scattering By Nonspherical Particles: Theory, Measurements, and Applications*, M. I. Mishchenko, J.W. Hovenier, and L. D. Travis (eds), pp. 309–322. Academic Press, San Diego, CA.

Mano, Y., 2000: Exact solution of electromagnetic scattering by a three-dimensional hexagonal ice column obtained with the boundary-element method. *Appl. Opt.* **39**, 5541–5546.

McFarquhar, G. M., A. J. Heymsfield, A. Macke, J. Iaquinta, and S. M. Aulenbach, 1999: Use of observed ice crystal sizes and shapes to calculate the mean-scattering properties and multispectral radiance; CEPEX April 4 1993 case study. *J. Geophys. Res.* **104**, 31763–31779.

Merewether, D. E., R. Fisher, and F. W. Smith, 1980: On implementing a numeric Huygen's source in a finite difference program to illuminate scattering bodies. *IEEE Trans. Nuclear Sci.* **27**, 1829–1833.

Meyer, K., P. Yang, and B.-C. Gao, 2004: Optical thickness of tropical cirrus clouds derived from the MODIS 0.66 and 1.38-μm channels. *IEEE Trans. Geosci. Remote Sens.* **42**, 833–841.

Mie, G., 1908: Beiträge zur Optik trüber medien, speziell kolloidaler Metalösungen. *Ann. Phy.* **25**, 377–445.

Miller, E. K., 1988, A selective survey of computational electromagnetics. *IEEE Trans. Antennas Propagat.* **36**, 1281–1305

Minnis, P., K. N. Liou and Y. Takano. 1993a: Inference of cirrus cloud properties using satellite-observed visible and infrared radiances. Part I: Parameterization of radiance fields. *J. Atmos. Sci.* **50**, 1279–1304.

Minnis, P., P. W. Heck and D. F. Young. 1993b: Inference of cirrus cloud properties using satellite-observed visible and infrared radiances. Part II: Verification of theoretical cirrus radiative properties. *J. Atmos. Sci.* **50**, 1305–1322.

Mishchenko, M. I., and A. Macke, 1998: Incorporation of physical optics effects and δ-function transmission. *J. Geophys. Res.* **103**, 1799–1805.

Mishchenko, M. I., and A. Macke, 1999: How big should hexagonal ice crystals be to produce halos? *Appl. Opt.* **38**, 1626–1629.

Mishchenko, M. I. and L. D. Travis, 1998: Capabilities and limitations of a current FORTRAN implementation of the T-matrix method for randomly oriented, rotationally symmetry scatterers. *J. Quant. Spectrosc. Radiat. Transfer* **60**, 309–324.

Mishchenko, M. I., W. B. Rossow, A. Macke, and A. A. Lacis, 1996: Sensitivity of cirrus cloud albedo, bidirectional reflectance and optical thickness retrieval accuracy to ice particle shape. *J. Geophys. Res.* **101**, 16973–16985.

Mishchenko, M. I., W. J. Wiscombe, J. W. Hovenier, and L. D. Travis, 2000: Overview of scattering by nonspherical particles, in *Light Scattering by Nonspherical Particles: Theory, Measurements, and Geophysical Applications*, M. I. Mishchenko, J. W. Hovenier, and L. D. Travis (eds), pp. 29–60, Academic Press, San Diago, CA.

Mishchenko, M. I., L. D. Travis, and A. A. Lacis, 2002: *Scattering, Absorption, and Emission of Light by Small Particles*. Cambridge University Press, Cambridge, UK.

Mitchell, D. L., Y. Liu, and A. Macke, 1996: Modeling cirrus clouds. Part II: Treatment of radiative properties. *J. Atmos. Sci.* **53**, 2967–2988.

Moore, T. G., J. G. Blaschak, A. Taflove, and G. A. Kriegsmann, 1988: Theory and application of radiation boundary operators. *IEEE Trans. Antennas Propagat.* **36**, 1797–1812.

Muinonen, K., 1989: Scattering of light by crystals: a modified Kirchhoff approximation. *Appl. Opt.* **28**, 3044–3050.

Muinonen, K., L. Lamberg, P. Fast, and K. Lumme, 1997: Ray optics regime for Gaussian random spheres. *J. Quant. Spectrosc. Radiat. Transfer* **57**, 197–205.

Mur, G., 1981: Absorbing boundary condition for the finite-difference approximation of the time-domain electromagnetic-field equations. *IEEE Trans. Electromagn. Compat.* **23**, 377–382.

Noel, V., H. Chepfer, G. Ledanois and P. H. Flamant, 2001: computation of a single-scattering matrix for nonspherical particles randomlay or horizontally oriented in space. *Appl. Opt.* **40**, 4365–4375.

Nousiainen, T., Muinonen, K., and Raisanen, P., 2003: Scattering of light by large Saharan dust particles in a modified ray optics approximation. *J. Geophys. Res.* **108**, D1, 4025. doi:10.1029/2001JD001277.

Oguchi, T., 1973: Scattering properties of oblate raindrops and cross polarization of radio waves due to rain: calculations at 19.3 and 34.8 GHz. *J. Radio Res. Lab. Jpn.* **20**, 79–118.

Ohtake, T., 1970: Unusual crystal in ice fog. *J. Atmos. Sci.* **27**, 509–511.

Peltoniemi, J. I., Lumme, K., Muinonen, K., and Irvine, W. M., 1998: Scattering of light by stochastically rough particles. *Appl. Opt.* **28**, 4088–4095.

Purcell, E. M. and C. R. Pennypacker, 1973: Scattering and absorption of light by nonspherical dielectric grains. *Astrophys. J.* **186**, 705–714.

Rolland, P., K.N. Liou, M.D. King, S.C. Tsay, and G.M. McFarquhar, 2000: Remote sensing of optical and microphysical properties of cirrus clouds using MODIS channels: methodology and sensitivity to assumptions. *J. Geophys. Res.* **105**, 11,721–11,738.

Rockwitz, K.-D., 1989: Scattering properties of horizontally oriented ice crystal columns in cirrus clouds, *Appl. Opt.* **28**, 4103–41110.

Roskovensky, J.K., and K.N. Liou, 2003: Detection of thin cirrus from 1.38 μm/0.65 μm reflectance ratio combined with 8.6–11 μm brightness temperature difference. *Geophys. Res. Lett.* **30**, 10.1029/2003GL018135, ASC 4-1–4-5.

Saxon, D. S., Lectures on the scattering of light, in *Proceedings of the UCLA International Conference on Radiation and Remote Sensing of the Atmosphere*, J. G. Kuriyan (ed), pp. 227–308. Western Periodicals, North Hollywood, CA.

Schelkunoff, S. A. (1943). *Electromagnetic waves*. D. Von Nostrand, New York.

Shlager, K. L., and J. B. Schneider, 1998: A survey of the finite-difference time domain literature, in *Advances in Computational Electromagnetics*, A. Taflove (ed), pp.

1–62. Artech House, Boston, MA.
Stamnes, J. J., and H. Heier, 1998: Scalar and elctromagnetic diffraction point-spread functions. *Appl. Opt.* **37**, 3612–3622.
Stephens, G. L., 1980a: Radiative properties of cirrus clouds in the infrared region. *J. Atmos. Sci.* **37**, 435–446.
Stephens, G. L., 1980b: Radiative transfer on a linear lattice: Applications to anisotropic ice crystal clouds. *J. Atmos. Sci.* **37**, 2095–2104.
Stephens, G. L., S.-C. Tsay, P. W. Stackhous, and P. J. Flatau, 1990: The relevance of the microphysical and radiative properties of cirrus clouds to climate and climate feedback. *J. Atmos. Sci.* **47**, 1742–1753.
Sullivan, D. M., O. P. Gandhi, and A. Taflove, 1988: Use of the finite-difference time-domain method in calculating EM absorption in man models. *IEEE Trans. Biomedical Engineering* **35**, 179–186.
Sun, W., and Q. Fu, 2000: Finite-difference time-domain solution of light scattering by dielectric particles with large complex refractive indices. *Appl. Opt.* **39**, 5569–5578.
Sun, W., Q. Fu, and Z. Chen, 1999: Finite-difference time-domain solution of light scattering by dielectric particles with perfectly matched layer absorbing boundary conditions. *Appl. Opt.* **38**, 3141–3151.
Taflove, A., 1980: Application of the finite-difference time-domain method to sinusoidal steady-state electromagnetic-penetration problems. *IEEE Trans. Electromagn. Compat.* **22**, 191–202.
Taflove, A., 1995: *Computational Electrodynamics: The Finite-Difference Time-Domain Method*. Artech House, Boston, MA.
Taflove, A. and M. E. Brodwin, 1975: Numerical solution of steady-state eletromagnetic scattering problems using the time-dependent Maxwell's equations. *IEEE Trans. Microwave Theory Tech.* **23**, 623–630.
Taflove, A., and S. C. Hagness (eds.), 2000: *Computational Electromagnetics*, 2nd edn. Artech House, Boston, MA.
Taflove, A., and K. R. Umashankar, 1990: The finite-difference time-domain method for numerical modeling of electromagnetic wave interactions with arbitrary structures. *Progress in Electromagnetic Research (PIER)* **2**, 287–333.
Takano, Y., and K. Jayaweera, 1985: Scattering phase matrix for hexagonal ice crystals computed from ray optics. *Appl. Opt.* **24**, 3254–3263.
Takano, Y., and K. N. Liou, 1989a: Solar radiative transfer in cirrus clouds. Part I. Single-scattering and optical properties of hexagonal ice crystals. *J. Atmos. Sci.* **46**, 3–19.
Takano, Y., and Liou, K. N., 1989b: Radiative transfer in cirrus clouds. II. Theory and computation of multiple scattering in an anisotropic medium. *J. Atmos. Sci.* **46**, 20–36.
Takano, Y., and K. N. Liou, 1995: Radiative transfer in cirrus clouds. III. Light scattering by irregular ice crystals. *J. Atmos. Sci.* **52**, 818–837.
Thuman, W. C., and E. Robinson, 1954: Studies of Alaskan ice-fog particles. *J. Meteor.* **11**, 151–156.
Umashankar, K. and A. Taflove, 1982: A novel method to analyze electromagnetic scattering of complex objects. *IEEE Trans. Electromagn. Compat.* **24**, 397–405.
van de Hulst, H. C., 1957: *Light Scattering by Small Particles*. John Wiley, New York.
Vinh, H., H. Duger, C. P. Van Dam, 1992: Finite-difference methods for computational electromagnetics(CEM). *IEEE AP-S International Symposium Digest* **3**, 1682–1683.

Wait, J. R., 1955: Scattering of a plane wave from a circular dielectric cylinder at oblique incidence. *Can. J. Phys.* **33**, 189–195.

Waterman, P. C., 1971: Symmetry, unitarity, and geometry in electromagnetic scattering, *Phys. Rev.* **D3**, 825–839.

Wendling, P., R. Wendling, and H. K. Weickmann, 1979: Scattering of solar radiation by hexagonal ice crystals. *Appl. Opt.* **18**, 2663–2671.

Wriedt, T., 1998: A review of elastic light scattering theories. *Part. Part. Syst. Charact.* **15**, 67–74.

Wylie, D. P., W. P. Menzel, H. M. Woolf, and K. I. Strabala, 1994: Four years of global cirrus statistics using HIRS. *J. Climate* **7**, 1972–1986.

Yang, P., and Q. Cai, 1990: Light scattering phase matrix for spheroidal and cylindric large particles. *Chinese J. of Atmos. Sci.* **14**, 345–358.

Yang, P., and K. N. Liou, 1995: Light scattering by hexagonal ice crystals: comparison of finite-difference time domain and geometric optics methods. *J. Opt. Soc. Amer. A* **12**, 162–176.

Yang, P., and K. N. Liou, 1996a: Finite-difference time domain method for light scattering by small ice crystals in three-dimensional space. *J. Opt. Soc. Amer. A* **13**, 2072–2085

Yang, P., and K. N. Liou, 1996b: Geometric-optics-integral-equation method for light scattering by nonspherical ice crystals. *Appl. Opt.* **35**, 6568–6584.

Yang, P., and K. N. Liou, 1997: Light scattering by hexagonal ice crystals: solution by a ray-by-ray integration algorithm. *J. Opt. Soc. Amer. A.* **14**, 2278–2288.

Yang, P., and K. N. Liou, 1998: Single-scattering properties of complex ice crystals in terrestrial atmosphere. *Contr. Atmos. Phys.* **71**, 223–248.

Yang, P., K. N. Liou, M. I. Mishchenko, and B.-C. Gao, 2000: An efficient finite-difference time domain scheme for light scattering by dielectric particles: application to aerosols. *Appl. Opt.* **39**, 3727–3737.

Yang, P., B.-C. Gao, B. A. Baum, W. Wiscombe, Y. Hu, S. L. Nasiri, A. Heymsfield, G. McFarquhar, and L. Miloshevich, 2001a: Sensitivity of cirrus bidirectional reflectance in MODIS bands to vertical inhomogeneity of ice crystal habits and size distributions. *J. Geophys. Res.* **106**, 17267–17291.

Yang, P., B.-C. Gao, B. A. Baum, W. Wiscombe, M. I. Mischenko, D. M. Winker, and S. L. Nasiri, 2001b: Asymptotic solutions of optical properties of large particles with strong absorption. *Appl. Opt.* **40**, 1532–1547.

Yang, P., B. A. Baum, A. J. Heymsfield, Y. X. Hu, H.-L. Huang, S.-Chee Tsay, and S. Ackerman, 2003: Single-scattering properties of droxtals. *J. Quant. Spectrosc. Radiat. Transfer* **79–80**, 1159–1180.

Yang, P., G. W. Kattawar, K.N. Liou, and J. Q. Lu, 2004a: Choice of Cartesian grid configurations for applying the finite-difference time domain method to electromagnetic scattering by dielectric particles. *Appl. Opt.* **43**, 4611–4624.

Yang, P., G. W. Kattawar, and W. J. Wiscombe, 2004b: Effect of particle asphericity on single-scattering parameters: comparison between Platonic solids and spheres. *Appl. Opt.* **43**, 4427–4435.

Yee, S. K., 1966: Numerical solution of initial boundary value problems involving Maxwell's equations in isotropic media. *IEEE Trans. Antennas Propagat.* **14**, 302–307.

Yee, S. K., J. S. Chen, and A. H. Chang, 1992: Conformal finite difference time domain (FDTD) with overlapping grids. *IEEE Trans. Antennas Propagat.* **40**, 1068–1075.

Zhai, P., Y.-K. Lee, G. W. Kattawar, and P. Yang, 2004: On the near to far field transformation for the finite-difference time domain (FDTD) application. *Appl.*

Opt. **43**, 3738–3746.

Zhang, Z., P. Yang, G. W. Kattawar, S.-C. Tsay. B. A. Baum, H.-L. Huang, Y. X. Hu, A. J. Heymsfield, and J. Reichardt, 2004: Geometrical-optics solution to light scattering by droxtal ice crystals. *Appl. Opt.* **43**, 2490–2499.